3

The Interior of Jupiter

Tristan Guillot
Observatoire de la Côte d'Azur, Nice

David J. Stevenson
California Institute of Technology

William B. Hubbard
Lunar and Planetary Laboratory, University of Arizona

Didier Saumon
Los Alamos National Laboratory

3.1 INTRODUCTION

Jupiter, owing to its large mass and rapid formation, played a crucial role in shaping the solar system as we know it today. Jupiter mostly contains hydrogen and helium (more than 87% by mass), and as such bears a close resemblance to the Sun. However, the Sun has only 2% of its mass in elements other than hydrogen and helium (the *heavy elements*), whereas Jupiter has between 3 and 13%. The exact amount of these heavy elements in the planet and their distribution are keys to understanding how the solar system formed.

Yet, it would seem that since the first Jupiter book was published, more than twenty five years ago, there has been little qualitative change to our vision of the interior of Jupiter, as a planet with a central dense core and a surrounding hydrogen and helium envelope (Stevenson and Salpeter 1976, Hubbard and Slattery 1976). Fortunately, several factors have led to significant quantitative improvements to that picture. Jupiter's gravity field has been measured with a better accuracy by the *Voyager* flybys in 1979, thereby yielding stronger constraints on the interior models. Our understanding of its atmosphere has been steadily improved, in particular by the in situ measurements of the *Galileo* probe in 1995, but also by the *Galileo* and *Cassini* missions, and by more accurate ground-based observations. On the experimental side, hydrogen (actually deuterium) has been successfully compressed to pressures up to several Mbar. Although the latest experiments remain controversial, this has generally led to the calculation of improved equations of state, a crucial ingredient for the calculation of interior models of the giant planet. Last but not least, the discovery of giant planets in orbit around other stars and of the related *brown dwarfs* has motivated more detailed studies of the evolution of substellar objects, with direct applications to Jupiter.

To first order, Jupiter's interior can be described by simple arguments. Jupiter is a hydrogen–helium planet in hydrostatic equilibrium. Its interior is warm ($\sim$20000 K) because it formed from an extended gas cloud whose gravitational energy was converted into heat upon contraction. (It is still contracting at the rate of $\sim$3 cm per year while its interior cools by $\sim$1 K per million year.) This has several important consequences: The relatively warm conditions imply that Jupiter's interior is *fluid*, not solid. The cooling and contraction yield a significant intrinsic energy flux (revealed by the fact that Jupiter emits more energy than it receives from the Sun) that drives convection in most parts of the interior. Convection ensures the planet's homogeneity and generates the observed magnetic field through a dynamo mechanism.

Were the above description entirely true, one would be able to derive the planet's composition directly from the determination of the atmospheric abundances. However, several factors contribute to a more complex picture of Jupiter's interior. As discussed in Section 3.2, the observation of the planet's atmosphere indicates that several major chemical species (such as helium, neon and water) are partly sequestered into the interior. In the interior, the degenerate nature of the electrons and the Coulomb interactions between ions can be responsible for phase transitions and/or phase separations, synonymous with chemical inhomogeneities (Section 3.3). Energy transport is complicated by the possibility of radiative transport of the intrinsic heat flux in some regions, while convection itself is complicated by the presence of molecular weight gradients and by intricate coupling with rotation and magnetic fields (Section 3.4). Finally, interior models based on the measurements of the planet's gravity field generally (but not always) require the presence of a central, dense core of uncertain mass and composition (Section 3.5). As shown in Section 3.6, this has major consequences for the planet's evolution and our understanding of its formation. Answering the most fundamental questions concerning Jupiter's origin (and by extension, the origin of the solar system) requires a renewed exploration of this planet.

Table 3.1. Characteristics of the gravity fields and radii.

Mass (total)	$1.898\,611\,2(15)\times10^{30}$ g	(a)
Equatorial radius (1 bar)	$7.1492(4)\times10^{9}$ cm	(b)
Polar radius (1 bar)	$6.6854(10)\times10^{9}$ cm	(b)
P_ω (magnetic)	$3.572\,97(41)\times10^{4}$ s	(c)
J_2 (1 bar)	$1.4697(1)\times10^{-2}$	(a)
J_4 (1 bar)	$-5.84(5)\times10^{-4}$	(a)
J_6 (1 bar)	$0.31(20)\times10^{-4}$	(a)

The numbers in parentheses are the uncertainty in the last digits of the given value. The value of the gravitational constant used to calculate the mass of Jupiter is $G = 6.672\,59 \times 10^{-8}$ dyn cm^2 g^{-1} (Cohen and Taylor 1987).
(a) Campbell and Synnott (1985)
(b) Lindal *et al.* (1981)
(c) Davies *et al.* (1986)

Table 3.2. Magnetic moments (in Gauss) for Jupiter and Saturn.

		Jupiter[a]		Saturn[b]	
n	m	g_n^m	h_n^m	g_n^m	h_n^m
1	0	4.208	0.	0.2144	0.
1	1	−0.660	0.261	−0.0014	0.0014
2	0	−0.034	0.	0.0188	0.
2	1	−0.759	−0.294	−0.0052	−0.0043
2	2	0.483	0.107	0.0050	−0.0004
3	0	...	0.	...	0.
3	1	...	...	...	...
3	2	0.263	0.695	...	...
3	3	−0.069	−0.247	...	...

[a] from Connerney *et al.* (1982)
[b] from Acuña *et al.* (1983)

3.2 AVAILABLE DATA

3.2.1 Gravity Field and Global Properties

Jupiter is a rapid rotator: its rotation period derived from its magnetic field is 9 h 55 m 29.71 s. A fluid body with an internal flow field that is purely zonal and symmetric about the equatorial plane will have a particularly simple gravity field of the form:

$$U(r,\theta) = \frac{GM}{r}\left\{1 - \sum_{i=1}^{\infty}\left(\frac{R_{\rm eq}}{r}\right)^{2i} J_{2i}P_{2i}(\cos\theta)\right\} \qquad (3.1)$$

where G is the gravitational constant, M the mass of the planet, $R_{\rm eq}$ its equatorial radius, r the distance to the planetary center, θ the colatitude and P_{2i} are Legendre polynomials. Current gravity field data show no detectable deviation from this assumed form. The J_{2i} are the gravitational moments. Their observed values (inferred mostly from the trajectories of the *Pioneer* and *Voyager* spacecrafts) are given in Table 3.1. The gravitational moments can also be related to the internal density profile $\rho(r)$ (and thus to theoretical models) by the following relation (e.g., Zharkov and Trubitsyn 1974):

$$J_{2i} = -\frac{1}{MR_{\rm eq}^{2i}}\int \rho(r) r^{2i} P_{2i}(\cos\theta)\, d\tau \qquad (3.2)$$

in which the integral is calculated over the total volume τ of the planet. A common method for the solution of Eq. (3.2) is the so-called theory of figures, which will not be developed here (see Zharkov and Trubitsyn 1978).

A special and important case for which Equation (3.1) is exactly true arises when the flow field depends at most on distance from the rotation axis. (The case of rigid rotation is a trivial example of this.) Deviations from rigid rotation will be small in a region of substantial electrical conductivity (Hide and Stannard 1976), and deviations from rigid rotation are likely to take the form of geostrophic flow (rotation on cylinders) elsewhere (Busse 1976). Symmetry-breaking flows such as convection are expected to be tiny by comparison (Stevenson and Salpeter 1977b). Most analyses of Jupiter's gravity assume rigid body rotation throughout.

Differential rotation is suggested by the observed atmospheric motions (e.g., Gierasch and Conrath 1993) as well as theoretical considerations (Busse 1976). The question of the depth to which these differential rotation patterns extend is still open. Hubbard (1982) has proposed a solution to the planetary figure problem in the case of a deep rotation field that possesses cylindrical symmetry. It is thus possible to derive, from interior models assuming solid rotation, the value of the gravitational moments that the planet would have if its surface rotation pattern extended deep into its interior. It is *a priori* impossible to prefer one model to the other. The correction due to differential rotation is of order -1.5×10^{-5} for J_2, $+4 \times 10^{-6}$ for J_4 and -10^{-6} for J_6. Due to the unknown rotation of the planet at deep levels, this correction has to be treated as an uncertainty (its value can be added to the measured moments given by Table 3.1 when theoretical models are calculated with equations valid for solid body rotation). (For further discussion of the influence of differential rotation on the external gravity field, see Section 3.5.4.)

3.2.2 Magnetic Field

The external magnetic field $\mathbf{B}$ is generally expressed as an expansion in spherical harmonics of the scalar potential W, such that $\mathbf{B} = -\nabla W$:

$$W = R_{\rm eq}\sum_{n=1}^{\infty}\left(\frac{R_{\rm eq}}{r}\right)^{n+1}\sum_{m=0}^{n}\{g_n^m\cos(m\phi) + h_n^m\sin(m\phi)\}\,P_n^m(\cos\theta) \qquad (3.3)$$

where ϕ is the longitude and the P_n^m are the associated Legendre polynomials. The coefficients g_n^m and h_n^m are the magnetic moments that characterize the field. They are expressed in magnetic field units (e.g., Gauss).

One can show that the first coefficients in Eq. (3.3) (for $m = 0$ and $n = 1$) correspond to the potential of a magnetic dipole such that $W = \mathbf{M}\cdot\mathbf{r}/r^3$ where M is the moment. As seen from Table 3.2, Jupiter and Saturn have magnetic fields of essentially dipolar nature, with a magnetic axis close to the rotation axis (g_1^0 is much larger than the other harmonics). Note that Uranus and Neptune have magnetic fields that are intrinsically much more complex. The magnetic dipolar moments are $M = 4.27\,\text{Gauss}\,R_{\rm J}^3$ for Jupiter, and $M = 0.21\,\text{Gauss}\,R_{\rm S}^3$ for Saturn. The dipole tilts (angle between the magnetic and rotation axis) are about 9.6° for Jupiter and less than 1° for Saturn (Connerney *et al.* 1982, Acuña *et al.* 1983).

It is thought likely that Jupiter's field, like Earth's field, is generated by a dynamo process, arising through convective motions in an electrically conducting deep interior. Although Jupiter's field is considerably larger than Earth's field, almost all other known aspects of the field are remarkably like those of Earth (Stevenson 1983). One obvious similarity is the dipole tilt. However, the similarity between the two fields runs much deeper. To appreciate this, it is important to "downward continue" the measured field to the level that one thinks represents the surface of the field generating region. If one chooses this to be at 0.75 to 0.8 Jupiter radii, and uses the known correct location for Earth (0.55 Earth radii, the top of Earth's core, seismologically determined) then the ratio of quadrupole to dipole and the ratio of octupole to dipole are the same for Jupiter and for Earth at the core "surface". In both cases, the quadrupole is suppressed, and this is characteristic of dipole family solutions to the dynamo generation of magnetic fields (Roberts and Glatzmeier 2000). The physical significance of the "core surface" for Jupiter is discussed in Section 3.5.3.

Comparison of spacecraft data over twenty-five years suggests that Jupiter's field may undergo secular variation with a timescale similar to that observed for Earth. However, the accuracy of earlier field models is sufficiently uncertain that no variation has been definitively observed (Russell *et al* 2001). The old ideas of westward drift are no longer accepted in the geomagnetic community as a sufficient explanation for the variation of Earth's field (Dormy *et al.* 2000) but it is believed that these field variations are indicative of the convective motions in the uppermost region of the planet in which the field is strongly coupled to the flow. For the largest variations suggested by Russell *et al* (2001), motions in Jupiter could be as much as an order of magnitude larger than those for Earth (merely because Jupiter's radius is an order of magnitude larger). This suggests motions of up to 0.1 to $1\,\mathrm{cm\,s^{-1}}$ and the significance of this is discussed further in Sections 3.4 and 3.5. Note, however, that this has no direct bearing on the important question of whether there are large, uniform zonal flows since they can only produce unobserved toroidal field.

Saturn's field is different from Jupiter's field in having no detectable dipole tilt. However, it has been suggested that this is an effect external to the region where the magnetic field is produced so that the deep-seated field of Saturn might be very similar to Jupiter (Stevenson 1980, 1982a). By contrast the fields of Uranus and Neptune are profoundly different. They have large dipole tilts and large quadrupole moments, which is suggestive of quadrupole family solutions of the dynamo equations.

3.2.3 Atmospheric Composition

The most important components of the atmosphere of Jupiter (as well as Saturn, Uranus and Neptune) are also among the most difficult to detect: H_2 and He have no electric dipolar moments, and mostly absorb during collisions. However, an accurate helium to hydrogen ratio is now available thanks to the in situ measurement by the *Galileo* probe (von Zahn *et al.* 1998, Chapter 2). The helium mole fraction (i.e., number of helium atoms over the total number of species in a given volume) is $q\mathrm{He} = 0.1359 \pm 0.0027$. The helium mass mixing ratio Y (i.e., mass of helium atoms over total mass) is obtained from $Y/(X + Y) = 0.238 \pm 0.005$, where X is the hydrogen mass mixing ratio. This value of Y is by coincidence very close to that of the Sun's atmosphere, but because of helium sedimentation in the Sun's radiative zone, Y was larger in the protosolar nebula: $Y_{\mathrm{proto}} = 0.275 \pm 0.01$ and $(X+Y)_{\mathrm{proto}} \approx 0.98$ (e.g., Bahcall and Pinsonneault 1995). Less helium is therefore found in the atmosphere of Jupiter than inferred to be present when the planet formed. The most natural explanation is a phase separation of helium in hydrogen and the subsequent formation of heavy helium-rich droplets falling to deeper levels under the action of gravity (see e.g., Stevenson and Salpeter 1977b for a detailed discussion). This explanation is also favored by the fact that neon which tends to dissolve into helium-rich droplets (Roulston and Stevenson 1995) is found to be significantly depleted in the atmosphere compared to the solar abundance (Niemann *et al.* 1998).

If the interpretation for helium is correct then there is a tendency for the atmosphere to become top heavy over time (i.e., the atmospheric material is more dense than the material located just *above* the helium separation region when compared at the same T and P). This will tend to promote mixing and homogenization to great depth, even if there is an intervening radiative zone (as discussed in 3.4). Consequently, the atmosphere is expected to provide a useful guide to the composition of a large fraction of Jupiter's volume.

The situation is more complex in the case of other elements because chemical and meteorological effects are sources of considerable heterogeneity in the atmosphere (see Chapters 4 and 5). Rather than trying to describe the many subtleties of Jupiter's chemistry, we will focus globally on all the elements other than hydrogen and hydrogen, i.e., the *heavy elements*: A surprising result of the *Galileo* probe is that within the error bars, carbon, sulfur, phosphorus, krypton, xenon and argon are all enriched relative to hydrogen by a factor $\sim$3 compared to the Sun's atmosphere (Mahaffy *et al.* 2000, Owen *et al.* 1999). The case of nitrogen is yet unclear but it may be consistent with this figure. Last but not least, oxygen is the most abundant atom in the universe after hydrogen and helium, but its abundance in Jupiter's deep atmosphere is still unknown, due to meteorological effects affecting the abundance of water. Interpretation of the water features in 5 micron spectra (which probe deeper levels than other spectral regions) indicate that the bulk abundance of oxygen is probably at least solar.

Assuming that heavy elements are uniformly enriched by a factor 3 over solar in Jupiter's interior, their total mass would amount to 18 $M_\oplus$. However, in a solar composition mixture, oxygen contributes up to half of the mass of heavy elements. The determination of its abundance should therefore be a critical goal of future space missions to Jupiter.

3.2.4 Energy Balance and Atmospheric Temperatures

As known since the infrared observations of Low (1966), Jupiter emits more energy than it receives from the Sun. This is the natural result of the cooling and contraction of the planet, as it slowly releases its primordial potential gravitational energy (see Hubbard 1968, 1977). Table 3.3 shows that about 40% of Jupiter's *infrared* flux is due to its intrinsic flux, the rest being due to the *absorbed* solar

Table 3.3. Energy balance and atmospheric temperatures[a].

Absorbed power	$5.014(248)\times10^{24}$ erg s^{-1}	
Emitted power	$8.365(84)\times10^{24}$ erg s^{-1}	
Intrinsic power	$3.350(260)\times10^{24}$ erg s^{-1}	
Intrinsic flux	5440(430) erg s^{-1} cm^{-2}	
Bond albedo	0.343(32)	
Effective temperature	124.4(3) K	
1-bar temperature	170.4(50) K	radio-occultation[b]
	166.1(4) K	hot spot[c]
22-bar temperature	427.7(12) K	hot spot[c]

[a] Hanel *et al.* (1981), see also Pearl and Conrath (1991)
[b] Lindal *et al.* (1981), adjusted (see text)
[c] Seiff *et al.* (1998)

flux (the directly reflected part is not included in the energy balance).

A crucial consequence of the presence of an intrinsic heat flux is that it requires high internal temperatures (~10 000 K or more), and that consequently Jupiter is *fluid* (not solid) (Hubbard 1968, see also Hubbard *et al.* 1995). Another consequence is that its interior is essentially convective with a temperature profile that is close to an *adiabat*. We will come back to this in more detail in Section 3.4.

Jupiter's deep atmosphere (more accurately troposphere) is indeed observed to be close to an adiabat, a result first obtained by Trafton (1967), but verified by radio-occultation experiments by the *Voyager* spacecrafts (Lindal *et al.* 1981), and by the in situ measurement from the *Galileo* probe (Seiff *et al.* 1998).

The atmospheric temperatures are important because they define the outer boundary condition of interior models. Such a boundary condition is often defined at the 1 bar level. The temperature retrieved from the *Voyager* data (radio-occultation and infrared spectra) led to a value of 165 ± 5 K (Lindal *et al.* 1981). However, this was using an incorrect helium to hydrogen ratio. Using the He/H value from *Galileo* (von Zahn *et al.* 1998) one finds that a reanalysis of the radio occultation data leads to a 1 bar temperature of 170.4 ± 5 K. On the other hand, the *Galileo* probe found a 1 bar temperature of 166.1 ± 0.4 K (Seiff *et al.* 1998). Horizontal temperature variations can only be measured down to pressures smaller than a fraction of a bar, and are of order ~5 K (Conrath *et al.* 1989).

The *Galileo* probe measurements indicate a temperature profile close to a *dry* adiabat down to 22 bar. However, the probe fell into a *hot spot*, a relatively rare, dry region of Jupiter's atmosphere. It is not clear that the measurements are also relevant outside hot spots. For example, the mean temperature profile could be closer to a *moist* adiabat (a more uniform temperature profile due to the release of latent heat by condensation), as for the Earth's atmosphere. In that case the planet's interior temperature would be colder by a factor that would depend almost linearly on the bulk abundance of water, i.e., about 0.5% for a solar abundance, 1% for a factor 2 enrichment in water...etc. Furthermore, because water is heavier than hydrogen, the reverse can also be true, i.e., a *superadiabatic* mean temperature profile, especially for large enrichments (see Guillot 1995). In that case, the interior temperature would be larger than expected. This can potentially affect the amount of heavy elements obtained from interior models: at fixed density profile, a higher temperature will be compensated by a larger amount of heavy elements. However, for most enrichments the effect is relatively small.

3.2.5 Tidal Response

The tidal distortion of Jupiter arising from the Galilean satellites has not yet been detected in the gravity field, because the largest (Io) tide would correspond to a gravity coefficient C_{22} of order 10^{-7}, even smaller than the measured $J_6 \sim 10^{-5}$. The corresponding real part of the Love number would tell us (independently of J_2) about the linear response of Jupiter to degree-two disturbances and may be readily detected in a future orbiter mission. However ,we have a long-standing constraint on the imaginary part of this Love number, directly related to the more commonly referenced tidal Q. The tidal Q is an inverse measure of the tidal dissipation, so that very high Q implies very low dissipation. From the requirement that the orbit of Io expands and the resonant heating of Io persists, we require $Q \sim 10^5$ (Goldreich and Soter 1966, Peale 1999). Unfortunately, there is no consensus yet on what this value tells us about the nature of Jupiter's interior.

A similar value appears to be needed to explain the tendency of extrasolar planets to have low eccentricity orbits at small semi-major orbital distances ($a \lesssim 0.07$ AU) from their central stars (e.g., Marcy *et al.* 1997). This could suggest that the cause of this Q is generally present in giant planets and perhaps not related to some "special" mechanism such as helium raindrops (Stevenson 1983b). On the other hand, contrary to Jupiter, extrasolar planets with short orbital periods develop a thick external radiative region (Guillot *et al.* 1996, Guillot and Showman 2002) in which tidal waves can be efficiently dissipated (Lubow *et al.* 1997). The discovery of a statistically significant number of extrasolar planets and their characterization (e.g., by transit detections) should shed light on the problem of tidal dissipation in giant planets. (For further discussion of Jupiter's tidal response to Galilean satellites, see Section 3.5.4.)

3.2.6 Oscillations

The case for the existence of free oscillations of the giant planets is still unresolved. Such a discovery would lead to great leaps in our knowledge of the interior of these planets, as can be seen from the level of accuracy reached by solar interior models since the discovery of its oscillations. At present, there is no clearly identified mechanism capable of exciting Jupiter's vibrations to an observationally detectable level. Turbulent convection, thought to be responsible for the Sun's oscillations (Goldreich and Kumar 1988) yields negligible amplitudes when applied to Jupiter (Deming *et al.* 1989). Other possibilities generally invoke the presence of stable regions (e.g., at the transition between molecular and metallic hydrogen) but are largely speculative. On the other hand, observations aimed at detecting modes of Jupiter have shown promising results (Schmider *et al.* 1991), but have thus far been limited by instrumental and windowing effects, and by the complex nature of the atmosphere (Lederer *et al.* 1995). Recent work by Mosser *et al.* (2000) puts

an upper limit to the amplitude of the modes at $0.6\,\mathrm{m\,s^{-1}}$, and shows increased power in the Fourier spectrum in the expected range of frequencies. Observations from space or from an Earth-based network of telescopes should be pursued in order to verify these results.

3.3 EQUATIONS OF STATE

The equation of state is the ensemble of equilibrium thermodynamic properties of a material, here taken to be a fluid mixture predominantly composed of hydrogen, helium, and a small amount of heavier elements. At the high pressures and moderate temperatures characteristic of Jupiter's interior, it is extremely challenging to study the equation of state either experimentally or theoretically. Yet, it is one of the most important factors in modeling Jupiter's structure and inferring its internal composition (Section 3.5.2). At low pressures and temperatures, in the outer regions of the planet, hydrogen is a molecular fluid. In the deep interior, where pressures of several tens of Mbar are achieved, the average distance between two neighboring nuclei is smaller than a Bohr radius. The electrons can no longer be bound to nuclei and the fluid is ionized. This warm, dense plasma is characterized by strong electron degeneracy and strong Coulomb interactions between the ions. These physical conditions are similar to those found in liquid metals and this plasma is often referred to as "liquid metallic hydrogen." The bulk of Jupiter is made of this material. The transitional regime where hydrogen goes from a mostly molecular fluid to the fluid metallic state is known as pressure ionization, a process of great significance to the interior of Jupiter but that remains poorly understood.

Equations of state used in modeling the interior of the planet are based on theoretical calculations involving various approximations that until recently had been largely untested in the appropriate regimes of pressure and temperature. Several recent experiments on hydrogen and deuterium now provide data in regimes of interest for modeling Jupiter and can constrain modeled equations of state. This renewed focus on hydrogen at Mbar pressures has so far spurred more controversy than resolved important questions.

3.3.1 Hydrogen: Summary of High-Pressure Experiments

The high pressures and high temperatures typical of the interiors of giant planets can be achieved in the laboratory by shock-compression of a small sample of material. The shock is typically generated by a hypervelocity impactor or by a powerful laser. Measuring the thermodynamic properties of the compressed sample is quite difficult since such dynamical experiments last only 5–100 ns and the sample can be very small (0.4–$500\,\mathrm{mm^3}$). For a given initial state of the sample, the family of shocked states that can be achieved follows a curve in the (P, ρ, T) phase diagram known as a Hugoniot. The Hugoniot is one of the Rankine–Hugoniot relations that result from the conservation of energy, momentum, and matter flux across the shock front. Nearly all dynamical experiments on hydrogen and deuterium performed share the same cryogenic initial state and therefore measurements from different experiments can be directly compared. By reflection of the shock wave on a back plate made of a material stiffer than the sample, a double-shocked state can be achieved that reaches even higher pressures with a modest increase in temperature. Multiple shock reflections, known as shock reverberation, lead to a succession of compressed states that approach adiabatic compression.

Since 1995, deuterium has been the subject of intense experimental study using several independent techniques.* Measurements of the pressure, density, temperature, reflectivity, electrical conductivity, and sound speed have been performed along the single-shock Hugoniot and, in some cases, along double-shock Hugoniots.

The most reliable experimental results come from experiments where the impactor is accelerated with a gas gun. This technique allows for larger samples ($\sim 500\,\mathrm{mm^3}$) and longer lasting (~ 100 ns) experiments but is generally limited to pressures below 1 Mbar. Pressures and densities have been measured along the single-shock Hugoniot up to 0.2 Mbar and along the double-shock Hugoniot up to 0.8 Mbar (Nellis *et al.* 1983). The reshocked states reproduce the (P, T) conditions of the molecular hydrogen envelope of Jupiter and provide a direct probe of the thermodynamics of hydrogen.

Under conditions where the dissociation of molecules becomes significant, the temperature becomes a sensitive test of the equation of state (EOS). Processes that can absorb substantial amounts of energy like dissociation and ionization result in relatively cool temperatures and higher degrees of compression for a given pressure along the Hugoniot. In the absence of such processes, the energy of the shock is expended mostly in the kinetic degrees of freedom with a corresponding increase in temperature. The temperature of double-shocked deuterium (Holmes, Ross and Nellis 1995) was found to be lower than all EOS predictions by about 30–40%, indicating that dissociation plays a more important role than predicted by contemporaneous models.

Finally, the sound speed has been measured along the Hugoniot in gas gun experiments up to 0.28 Mbar (N. C. Holmes, private communication). Since it is a derivative of the pressure, the sound speed is a sensitive test of EOS models with the advantage of being measurable very reliably.

With powerful lasers, deuterium can be shocked to much higher pressures than with gas guns but the small sample size and the very short duration of the experiments make accurate diagnostics very challenging. The (P, ρ, T) single-shock Hugoniot has been measured recently up to 3.5 Mbar with the NOVA Laser Facility (Da Silva *et al.* 1997, Collins *et al.* 1998, Collins *et al.* 2001), reaching a maximum density of $\sim 1\,\mathrm{g\,cm^{-3}}$ at ~ 1 Mbar (Figure 3.1). Such a high compressibility was not anticipated by most EOS models and this work sparked the current interest in the thermodynamics of warm dense hydrogen as well as controversy, both on the theoretical and experimental fronts. The reflectivity of shocked deuterium reaches about 60% for pressures above 0.5 Mbar along the Hugoniot (Celliers *et al.* 2000), a value indicative of a large density of free electrons and of a high electric conductivity characteristic of fluid metallic hydro-

* Due to its higher density, deuterium is experimentally more advantageous than hydrogen because higher shock pressures can be achieved for a given impactor speed.

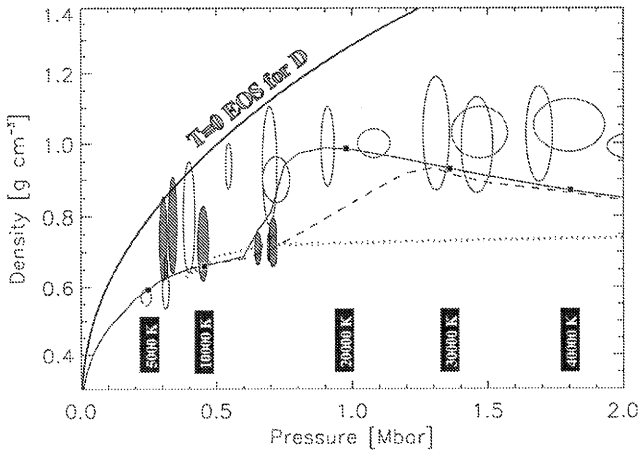

Figure 3.1. Comparison of experimental data and theoretical Hugoniot for deuterium (densities are twice larger than expected for hydrogen at any given pressure). Empty ellipses correspond to data points obtained from laser compression (Collins *et al.* 1998). Filled ellipses were obtained by magnetic compression (Knudson *et al.* 2001). Theoretical calculations are represented by lines. They are respectively: the "PPT" (solid) and "interpolated" (dashed) Saumon–Chabrier equations of state (Saumon, Chabrier and Van Horn 1995), and a Path Integral Monte Carlo EOS (dotted; Militzer and Ceperley 2000). The solid line to the left shows the T=0 equation of state for D_2 as determined by an exp-6 potential fit to diamond-anvil cell measurements (Hemley *et al.* 1990). The temperatures along the Hugoniot have been calculated using the PPT-EOS.

gen. Second-shock compression up to 6 Mbar with the Nike laser give results in agreement with the NOVA (P, ρ) data (Mostovych *et al.* 2000). On the other hand, Knudson *et al.* (2001) used a magnetic Z-accelerator to accelerate impactors to very high velocities. Their single-shock Hugoniot agrees well with the NOVA data for $P \lesssim 0.4$ Mbar but it is not as compressible at higher pressures, reaching a density of only $\sim 0.7\,\mathrm{g\,cm^{-3}}$ at 0.7 Mbar (Figure 3.1).

3.3.2 Hydrogen: EOS Calculations

While the temperatures obtained along the single-shock Hugoniot rapidly become much higher than those inside Jupiter at the same pressure (Figure 3.2), these measurements provide very important, and heretofore unavailable tests of equations of state in the 0.5 to 5 Mbar range where pressure ionization of hydrogen occurs. Conversely, EOS models can be used to compute the various physical quantities measured in the lab and to interpret the experimental results.

Theoretical single-shock Hugoniots computed from a wide variety of EOS models basically fall into two groups. First principle calculations (e.g., Militzer and Ceperley 2000, Lenosky *et al.* 1997, 2000, Galli *et al.* 2000) all predict a rather stiff Hugoniot that is in general agreement with the Z-accelerator data of Knudson *et al.* (2001). This is illustrated in Figure 3.1 by the Path Integral Monte Carlo calculation of Militzer and Ceperley (2000). On the other hand, models that are partly calibrated with experimental data (Saumon, Chabrier and Van Horn 1995, Ross 1998, Saumon *et al.* 2000, Ross and Yang 2001), obtain a generally good agreement with the NOVA data (Figure 3.1, Collins *et al.* 1998). Interestingly, the standard SESAME EOS of deuterium (Kerley 1972) predicts a Hugoniot that generally agrees with the much more sophisticated *ab initio* calculations.

Our study of a number of theoretical Hugoniots shows that EOS that have been fitted to the gas gun single- and double-shock (P, ρ, T) data of Nellis *et al.* (1983) and Holmes *et al.* (1995) – all taken below 0.8 Mbar and 5300 K – reproduce the high compression of the NOVA data (Collins *et al.* 1998) and the sound speed data along the single shock (N. C. Holmes, private communication). On the other hand, the first-principle calculations generally agree with the stiffer Hugoniot of Knudson *et al.* (2001) and cannot reproduce the high compression of the NOVA data. They also fail to reproduce the double-shock temperatures and the sound speed measurements. Some of the *ab initio* calculations disagree with the low-pressure gas gun data (e.g., Lenosky *et al.* 2000). On the one hand, the Knudson *et al.* (2001) data and nearly all first-principle EOS calculations are in good agreement with each other. On the other hand, more heuristic EOS models clearly show that four independent EOS experiments (second-shock temperature, sound speed, the NOVA single shock and the Nike double shock) are fully consistent with each other but neither with first principle calculations nor the Knudson *et al.* (2001) data. Both the high compressibility of the NOVA Hugoniot and the low gas-gun reshock temperatures can be explained by the absorption of the shock energy resulting from molecular dissociation.

This polarization of EOS calculations along different data sets has created a lively debate and is stimulating much additional (and challenging) experimental and theoretical work. The EOS of hydrogen in the 0.5 to 5 Mbar regime, where it is transformed from an insulating molecular fluid to a conducting liquid metal remains uncertain to a level that is significant for modeling the interior of Jupiter. The recent progress in this area has been very beneficial, however, as it appears that the current data and models bracket the actual EOS of hydrogen.

In order to model Jupiter's interior with confidence, a careful study of the uncertainties arising from the EOS would be required. This is not presently available, but Figure 3.1 shows that this can be crudely approximated by using the "interpolated" and the "PPT" equations of state of Saumon, Chabrier and Van Horn (1995) even though they do not fit the experimental data well. A comparison of Figures 3.1 and 3.3 shows that large uncertainties in density along the Hugoniot at 1 Mbar (~30%) result in much smaller differences along the Jupiter adiabat (~8%). The effects on the inferred core mass and the mass of heavy elements in Jupiter are discussed in Section 3.5.2.

A Plasma Phase Transition?

We have seen that hydrogen undergoes a transition from a low-pressure molecular insulating fluid to a high-pressure conductive fluid. Is the transition continuous, as is the case for temperature ionization, or rather a first order phase transition (the so-called *Plasma Phase Transition*, or PPT) with discontinuities in density and entropy across the coexistence curve? Such a first-order transition was first suggested by Wigner and Huntington (1935) on the basis of the different nature of the interaction potentials in metals (a weakly

repulsive, screened Coulomb potential) and in insulators (a strongly repulsive "hard-sphere" potential).

The PPT has not been observed experimentally in hydrogen (i.e., there is no evidence for the expected discontinuities), but it can be argued that the gas-gun experiments have not reached high enough pressures, and that laser-shocks may be supercritical. Note for example that using the new data, the critical point for the PPT computed by Saumon *et al.* (2000) is lower ($T \approx 14600$ K, $P \approx 0.73$ Mbar) than shown in Figure 3.2. The PPT is predicted by some of the more heuristic "chemical picture" EOS models (Saumon *et al.* 1995 and references therein) and Beule *et al.* (1999). On the other hand, none of the first-principle EOS calculations show evidence for a first order phase transition in warm dense hydrogen.

If present, the PPT would have significant consequences for the structure of Jupiter, Saturn, and low-entropy extrasolar giant planets. Its main effect would be to create an impenetrable barrier for convection between the molecular and metallic hydrogen parts of the envelope, affecting the mixing of chemical species (Stevenson and Salpeter 1977b). The thermodynamic conditions of phase equilibrium imply that the chemical composition across the PPT must be discontinuous (Landau and Lifschitz 1969), with the consequence that atmospheric abundances of all elements would no longer be indicative of their bulk abundance in the planet. In addition, as the planet cools, a fraction of the mass of the envelope is converted from one phase to the other with an associated latent heat release (or absorption). The effect on the evolution is not very pronounced for a latent heat of $\sim 0.5 k_B$ per proton (Saumon *et al.* 1992).

3.3.3 Helium: Emphasis on the H–He Phase Diagram

In comparison with hydrogen, the EOS of helium under the conditions of interest for Jupiter has been little studied. Single-shock Hugoniot data is available up to 0.56 Mbar (Nellis *et al.* 1984) only. The current controversy surrounding the hydrogen EOS suggests that untested EOS calculations of warm dense helium should be viewed with caution. A much more difficult problem is that of the phase diagram of H/He mixtures. Nevertheless, its importance in giant planets is such that this topic deserves a detailed discussion.

As first proposed for Jupiter and Saturn by Smoluchowski (1967) and Salpeter (1973), hydrogen and helium mixtures can undergo a *phase separation*: at low temperatures, helium (or other elements) can become insoluble and form helium-rich droplets. Under the action of gravity, these droplets will tend to fall toward the central regions of the planet.

Physically, a phase separation arises in a binary mixture of concentration x when the second derivative of the Gibbs free energy $\partial^2 G/\partial x^2 < 0$. The two concentrations x_1 and x_2 that correspond to phase equilibrium between the droplets and their surroundings are given by the equality of the chemical potentials:

$$\left.\frac{\partial G}{\partial x}\right|_{x_1} = \left.\frac{\partial G}{\partial x}\right|_{x_2}$$

The lower the temperature, the closer x_1 and x_2 are to 0 and 1, respectively.

The calculation of the miscibility of hydrogen and helium requires a knowledge of the (non-ideal) EOS of each element and, of course, of the interactions between hydrogen and helium species. Given the difficulty in modeling the EOS for hydrogen alone, it may not be so surprising that the question of the helium phase separation in the giant planets is still unsolved.

One approach has been to calculate the hydrogen-helium phase diagram assuming complete ionization. In that case, critical temperatures of order 8000 K at 2 Mbar can be calculated (Stevenson 1982b). Even more importantly, this leads to a critical temperature that *decreases* with increasing pressure. The consequence is that (i) this would imply that a phase separation has occurred in Jupiter, and earlier in Saturn, as suggested by the abundance of helium measured in the atmosphere (see Section 3.2.3), (ii) helium would be most insoluble near the molecular/metallic transition. Results from that approach (Hubbard and DeWitt 1985) are illustrated in Fig. 3.2 by two lines labelled ($Y = 0.21$ and $Y = 0.27$). These lines represent, in the liquid metallic-hydrogen phase, the limiting He mass fraction Y for a single-phase H–He solution.

Other calculations have been attempted in the local density approximation. Earlier work (Klepeis *et al.* 1991) suggested an unrealistically high critical temperature (40 000 K at 10.5 Mbar). However, a more careful study by Pfaffenzeller *et al.* (1995) with the same basic technique led to a lower critical temperature (less than 5000 K at 4 Mbar). This value would imply no demixing of helium in Jupiter and Saturn. More importantly, the work of Pfaffenzeller *et al.* implies a critical temperature that *increases* with pressure. This can be explained if hydrogen is still not fully ionized at the pressures considered (4 to 24 Mbar), which seems difficult to reconcile with the more standard hydrogen EOSs. Another problem of the work of Pfaffenzeller *et al.* is that it does not recover the fully ionized limit. If the critical temperature increases with pressure, this would open the possibility that helium separates from hydrogen over an extended fraction of the planetary radius, with significant consequences for the interior and evolution models.

An alternative approach is to constrain the phase diagram by requiring that evolution models for both Jupiter and Saturn yield a cooling time that agrees with the age of the solar system, 4.55 Ga. Recent calculations (Fortney and Hubbard 2003) indicate that the phase diagram shown on Fig. 3.2 implies only a modest differentiation of helium in Saturn, and a cooling time that is short of the required one by $\sim$1 Ga. However, Fortney and Hubbard propose that a slight modification of the phase diagram is sufficient to obtain the required cooling time: The solubility of He in an electron gas goes approximately as $x \sim \exp(-\Delta G/kT)$, where x is the concentration of He and ΔG is the Gibbs energy of immersion of the helium atom (Hubbard and Stevenson 1984). The results of Hubbard and DeWitt (1985) can be well represented by $\Delta G \sim 1.4$ eV at the pressures in Jupiter or Saturn near the PPT coexistence curve (Figure 3.2). Increasing ΔG by a factor $\sim$2 yields the correct age for Saturn, and at the same time has no effect on Jupiter, for which interior temperatures lie above the solar-composition line on Figure 3.2. However, this approach has limitations inherent to the uncertainties of the evolution calculations (see Section 3.6).

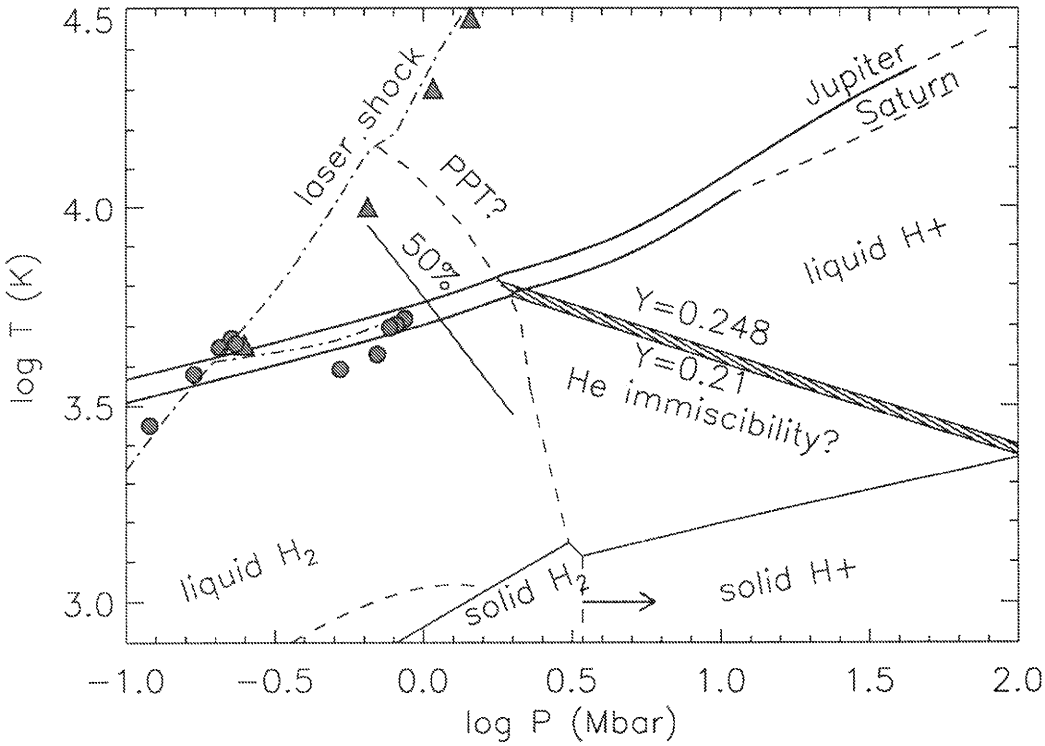

Figure 3.2. Hydrogen phase diagram, with interior profiles of present-day Jupiter and Saturn overlaid, and with some experimental data shown. The boundary between liquid H_2 and solid H_2 is somewhat uncertain in the Mbar pressure range (2 estimates are shown), but is not relevant to Jupiter. The laser-shock measurements of Collins *et al.* (2001) and the gas-gun measurements of Holmes *et al.* (1995) are shown as triangles and filled circles in the upper left-hand corner, respectively. Single- and double-shock hydrogen Hugoniots calculated by Saumon *et al.* (2000) are shown as dot-dashed lines in the same region of the plot. The solid line labeled "50%" shows where 50% of molecular dissociation is obtained in the model of Ross (1998).

Clearly, physical and astrophysical constraints on the hydrogen/helium phase diagram are consistent with a scenario in which the phase separation has begun recently in Jupiter, and a few billion years ago in Saturn due to its colder interior. However, the uncertainties on both constraints are significant, and a more detailed test of this scenario must await (i) an accurate understanding of the pressure ionization of hydrogen alone and (ii) calculations and experiments predicting the behavior of hydrogen–helium mixtures at Mbar pressures.

3.3.4 Heavy Elements

Due to their small molecular abundances, an approximate treatment of the equations of state of heavy elements is generally sufficient for the calculation of Jupiter's internal structure. However, the derivation of the amount of heavy elements present in the planet depends on the accuracy of these equations of state. Heavy elements also have indirect but crucial contributions, such as in calculating radiative opacities, and the possible existence of molecular weight gradients.

Figure 3.3 shows adiabats and isotherms for various elements and mixtures. The EOSs for the simplest elements, hydrogen and helium, yield density profiles with an inherent uncertainty of about 10% (the uncertainty due to the temperature profile being only a few percent). Other elements are roughly categorized into "ices" (elements which condensed in the protosolar nebula at temperatures $\sim$150 K, including water, ammonia, methane), and "rocks" (a mixture of more refractory materials). Polynomial fits to the pressure–density profiles for both kinds of mixtures have been calculated by Hubbard and Marley (1989) on the basis of experimental measurements (Nellis *et al.* 1997 and references therein). These are shown in Fig. 3.3. Note that these relations are independent of temperature. Thermal perturbations can be included by adding a thermal pressure component, which can be approximated by $P_{\rm therm} \approx 3\gamma\rho kT/m$, where k is Boltzmann's constant, m is the molecular mass and γ the Gruneisen parameter (e.g., Zharkov 1986). For $T \approx 10^4$ K, $m \approx 20$ amu, $\rho \approx 2\,{\rm g\,cm^{-3}}$, $\gamma \approx 1$, one finds $P_{\rm therm} \approx 0.3$ Mbar. Thermal effects can be neglected in the metallic region only. The most important source of uncertainty is the unknown composition of the heavy elements.

Water is especially important because it should contribute to about half of the mass of heavy elements if the ratios of elemental abundances to that of oxygen (e.g., C/O, N/O, Fe/O, ..., etc.) remain approximately solar. Experimental results on H_2O, as indicated by asterisks in Fig. 3.3 (Chau *et al.* 2001) are in good agreement with theoretical zero-temperature estimates by Zharkov and Trubitsyn (1978), but rules out the commonly used ANEOS H_2O equation of state which predicts densities that are systematically smaller than the laboratory measurements by $\sim$8%. The relatively good agreement between experiments and one theoretical prediction should however not occult two important

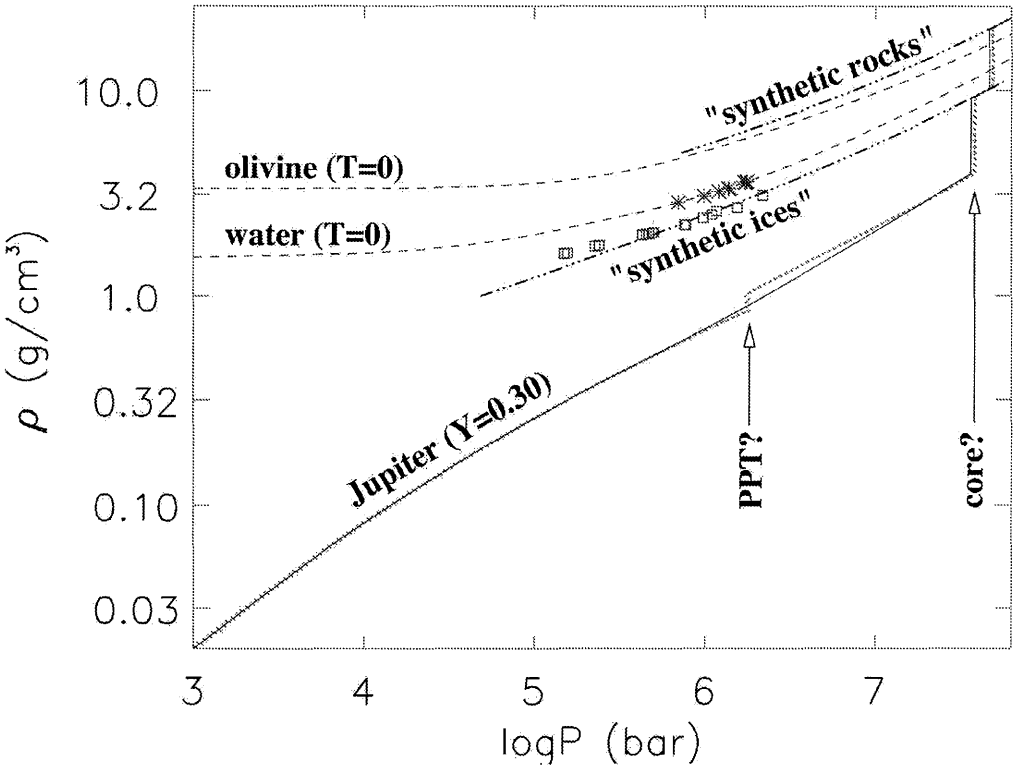

Figure 3.3. Comparison of density profiles: *Solid line*: Jupiter model with a pure hydrogen-helium envelope (X=0.70; Y=0.30) and a central ice/rock core, using the Saumon–Chabrier "interpolated EOS" (Saumon *et al.* 1995). *Dotted line*: *Idem* with the "PPT" SC EOS for hydrogen (see text). *Dashed lines*: Theoretical zero-temperature EOSs for ice VII (Zharkov and Trubitsyn 1978) and olivine (ANEOS). *Dash-dotted lines*: Analytic fits of Hubbard and Marley (1989) to experimental results of adiabatic compression of "synthetic ices" (a mixture of water, methane and ammonia) and "synthetic rocks" (a mixture of SiO_2, MgO, FeS and FeO). *Asterisks*: Shock-reverberation measurements for H_2O (Chau *et al.* 2001). *Squares*: Single- and double-shock measurements for "synthetic ices" (Nellis *et al.* 1997).

unknowns: (i) when does water metallize? (ii) how soluble is it in hydrogen? The first is important because water could provide a significant amount of electrons if its metallization takes place at low pressures. The second could limit the amount of water in the external envelope and create an inner "water-rich" region (this is possible for large enrichments of water over the solar value).

Globally, heavy elements are thought to be uniformly mixed throughout the hydrogen–helium envelope because of convection (next section). A phase separation can be important for mixtures with large enough abundances (helium and possibly water)[†]. Other factors can also affect the distribution of elements in Jupiter's interior in a more limited way. The dissolution of neon in helium raindrops (Roulston and Stevenson 1995) is one example, but other elements could also dissolve in liquid silicate raindrops, thought to form clouds at temperatures $T \sim 2000\,\mathrm{K}$ and $P \sim 10\,\mathrm{kbar}$ (a region where non-ideal effects are important). This partitioning could affect atmospheric abundances. Another crucial problem is the delivery of planetesimals at depths that depend on their composition (Podolak *et al.* 1988) and their subsequent mixing. Depending on the formation mechanisms and efficiency of convection, Jupiter's envelope could have either a solar ice to rock ratio, or be depleted in refractory material.

[†] This is due to the fact that, as discussed in the case of helium, given x the concentration of a minor species in hydrogen, a phase separation occurs when $T \lesssim -\Delta G/(k \ln x)$. For chemical species with a small abundance x, the Gibbs energy of immersion ΔG would need to be unrealistically large for demixing to occur.

3.4 TRANSPORTING JUPITER'S INTRINSIC HEAT

3.4.1 Radiation and Conduction

The fact that Jupiter emits more energy than it receives from the Sun implies that internal heat is transported from the planet's central region to space. The structure of the interior and the planet's evolution are intimately related to the mechanisms that transport this heat. Radiation and conduction can be modeled with the same approach. In the diffusion approximation (which assumes that the radiation field is isotropic, a very good hypothesis at the deep levels considered here), one defines a radiative gradient as:

$$\nabla_{\mathrm{rad}} = \frac{3}{16}\frac{\kappa P}{g}\left(\frac{T_{\mathrm{eff}}}{T}\right)^4 \tag{3.4}$$

where P is the pressure, κ the Rosseland opacity (including contributions due both to radiation and conduction), g is the gravity T_{eff} the effective temperature at the level considered ($\sigma T_{\mathrm{eff}}^4$ is the intrinsic energy flux), and T the temperature.

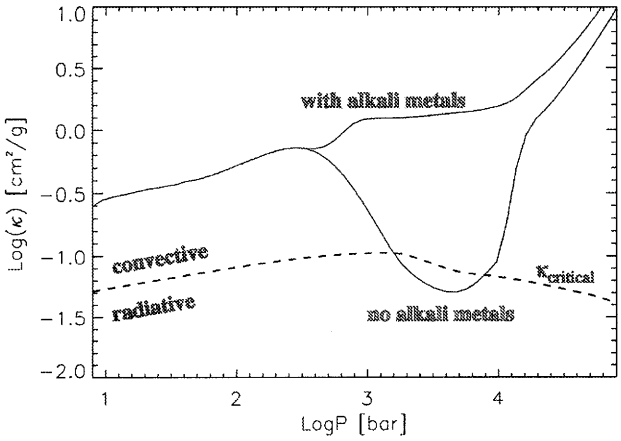

Figure 3.4. Comparison of Rosseland mean opacities (*solid lines*) along a model of Jupiter to the critical opacity (*dashed line*) above which the medium is convectively unstable (Schwarzschild's criterion). The opacity calculations assume a three times solar enrichment in heavy elements. Depending on the presence of alkali metals, Jupiter is found to be fully convective or to possess a small, deep radiative zone.

The *critical opacity* $\kappa_{\rm crit}$ is defined as the (Rosseland) opacity above which the medium is too opaque/resistant to transport the totality of the heat flux by radiation/conduction, and becomes convective. In a homogeneous inviscid mixture, this occurs when $\nabla_{\rm rad} > \nabla_{\rm ad}$, where $\nabla_{\rm ad} \equiv (\partial \ln T/\partial \ln P)_S$ is the adiabatic gradient. Assuming furthermore that g, $T_{\rm eff}$ and the temperature gradient $\nabla_T \equiv d\ln T/d\ln P$ are independent of depth, one finds that

$$\kappa_{\rm crit} \approx 8\nabla_{\rm ad}\kappa_0 \left(\frac{P}{P_0}\right)^{4\nabla_T - 1} \tag{3.5}$$

where we have introduced an equivalent opacity $\kappa_0 = (2/3)(g/P_0)$, and P_0 is for example the pressure at the tropopause.

Since $\nabla_T \approx 0.3$ in Jupiter, $\kappa_{\rm crit}$ is only weakly dependent on the level considered. However the opacity itself (in $\rm cm^2\,g^{-1}$) is a strong function of P and T. At pressures of a bar or more and relatively low temperatures (less than 1000 K), the three dominant sources of opacities are water, methane and collision-induced absorption by hydrogen molecules. Except possibly in limited regions ($P \lesssim 10$ bar) where meteorology due to water condensation can affect chemical abundances and/or yield a stable stratification (see discussion hereafter), Fig. 3.4 shows that convection is ensured by the rapid rise of opacity with increasing pressure. (Note that the critical opacity shown by a dashed line also slowly increases in regions where $\nabla_T > 0.25$).

However, in the intermediate temperature range between ~1200 and 1500 K, the Rosseland opacity due to the hydrogen and helium absorption behaves differently: the absorption at any given wavelength increases with density, but because the temperature also rises, the photons are emitted at shorter wavelengths, where the monochromatic absorption is smaller. As a consequence, the opacity can decrease. This was shown by Guillot *et al.* (1994a,b) to potentially lead to the presence of a deep radiative zone in the interiors of the giant planets.

This problem must however be reanalyzed in the light of recent observations and analyses of brown dwarfs. Their spectra show unexpectedly wide sodium and potassium absorption lines (see Burrows, Marley and Sharp 2000) in spectral regions where hydrogen, helium, water, methane and ammonia are relatively transparent. It thus appears that the added contribution of these elements (if they are indeed present inside Jupiter) would wipe out any radiative region at these levels (Guillot, Freedman, Lodders and Marley, in preparation). Figure 3.4 shows that opacities calculated without the contribution of these alkali metals present a marked dip, whereas those including them in the mixture do not, in which case the planet is expected to be fully convective. However the presence of alkali metals in Jupiter depends on the history of the formation of the planet. Although these elements are probably present, one could imagine that they can be retained in the central core of the planet and be under-abundant in the envelope.

At temperatures above 1500 ~ 2000 K two important sources of opacity appear: (i) the rising number of electrons greatly enhances the absorption of H_2^- and H^-; (ii) TiO, a very strong absorber at visible wavelengths, is freed by the vaporization of $CaTiO_3$. Again, the opacity rises rapidly which ensures a convective transport of the heat. Still deeper, conduction by free electrons becomes more efficient, but the densities are found not to be high enough for this process to be significant, except perhaps near the central core (see Hubbard 1968, Stevenson and Salpeter 1977a).

3.4.2 Convection

Modeling convection in the presence of rapid rotation, of a powerful magnetic field and of compositional gradients, is of extreme complexity. Fortunately, we are often mostly interested in order-of-magnitude estimates of two quantities: the superadiabatic temperature gradient necessary to transport the intrinsic heat flux, and the mean convective velocity. Rotation and magnetic field can significantly affect the type of convective style and fluid velocities, but it is useful to look first at the commonly used crude approximation provided by mixing length theory:

$$\nabla_T - \nabla_{\rm ad} \sim \left[\frac{4\sqrt{2}}{\alpha^2\delta^{1/2}}\frac{F_{\rm conv}}{c_P T(\rho P)^{1/2}}\right]^{2/3} \tag{3.6}$$

$$v_{\rm conv} \sim \left[\frac{\alpha\delta}{4}\frac{P}{\rho c_P T}\frac{F_{\rm conv}}{\rho}\right]^{1/3} \tag{3.7}$$

where $\alpha \sim 1$ is the mixing length parameter, $\delta = -(\partial \ln\rho/\partial\ln T)_P$, and c_P is the specific heat at constant pressure. The convective flux is $F_{\rm conv} = F(1 - \nabla_T/\nabla_{\rm rad})$, where F is the total flux. In our case, the opacities become rapidly large, therefore $\nabla_{\rm rad} \gg \nabla_T \approx \nabla_{\rm ad}$ and $F_{\rm conv} \approx F$. Physically, the superadiabatic gradient $\nabla_T - \nabla_{\rm ad}$ depends on the ratio of the energy per unit mass $F/\sqrt{\rho P}$ to be transported to that of a given layer, $c_P T$. The convective velocity is essentially proportional to $(F/\rho)^{1/3}$: since F is a slowly varying function, $v_{\rm conv}$ should be expected to be larger near the surface, where ρ is smaller. This corresponds to the fact that in a low density material, transporting the same energy requires higher velocities.

Values typical for Jupiter's interior yield the following quantitative expressions for the superadiabatic gradient and

Table 3.4. Properties of convection in Jupiter (order of magnitude estimates from the mixing length theory).

	P [bar]	T [K]	H_P [km]	$\nabla_T - \nabla_{ad}$	v_{conv} [$m\,s^{-1}$]	τ_{conv} [yrs]	ν [$m^2\,s^{-1}$]	$Pr = \frac{\nu}{\kappa}$	$Re = \frac{vd}{\nu}$	$Ro = \frac{v}{\omega d}$	$E = \frac{\nu}{\omega d^2}$
Atmosphere	1	165	20	10^{-5}	1	10^{-3}	10^{-5}	10^{-4}	10^{9}	0.4	10^{-10}
Molecular region	5×10^5	5100	3000	2×10^{-9}	0.1	1	10^{-6}	10^{-1}	10^{11}	10^{-4}	10^{-15}
Metallic region	4×10^6	8400	8000	4×10^{-10}	0.1	2	3×10^{-7}	10^{-2}	10^{12}	10^{-4}	10^{-16}
Core interface	4×10^7	20000	30000	5×10^{-11}	0.03	20	10^{-6}	10^{-2}	10^{12}	10^{-5}	10^{-17}

convective velocity:

$$\nabla_T - \nabla_{ad} \sim 2 \times 10^{-9} \left(\frac{H_p}{10^8\,\mathrm{cm}}\right)^{-1/3} \left(\frac{\rho}{1\,\mathrm{g\,cm^{-3}}}\right)^{-2/3} \times \left(\frac{T}{10^3\,\mathrm{K}}\right)^{-2/3} \left(\frac{F_{conv}}{10^3\,\mathrm{erg\,cm^{-2}\,s^{-1}}}\right)^{2/3}$$

$$v_{conv} \approx 20 \left(\frac{\nabla_T - \nabla_{ad}}{10^{-8}}\right)^{1/2} \left(\frac{H_p}{10^8\,\mathrm{cm}}\right)^{1/2} \mathrm{cm\,s^{-1}}$$

As shown in Table 3.4 the temperature gradient in the convective zone is thus almost indistinguishable from the adiabatic gradient. The velocities derived are relatively small (for example, they allow helium droplets to grow and fall before they can be transported efficiently, Stevenson and Salpeter 1977b), yet the convective timescale is always much shorter than the evolution timescale.

A few dimensionless numbers characterize convection itself and are given in Table 3.4, based on values of viscosities and conductivities from Stevenson and Salpeter (1977a), and radiative diffusivities as discussed in the previous section. These values are only order of magnitude estimates. As shown by the relatively small values of the *Prandtl* number, radiation (near the upper layers) and conduction (in the metallic interior) generally dominate over the microscopic diffusion of heat. However, the large *Reynolds* number shows the overwhelming importance of macroscopic diffusion, and the inherently turbulent nature of convection inside the planet. The low *Rossby* number indicates that rotation will significantly affect convective motions, implying that in the planet's interior, convective motions will be mostly confined to a plane perpendicular to the axis of rotation. (Note that *horizontal* motions in the atmosphere are characterized by $Ro \ll 1$ because the characteristic length is then $d \gg H_P$.) Finally, the *Ekman* number describes the relative magnitude of viscous and Coriolis forces. It is extremely low, indicating that frictional forces are largely negligible for large scale motions in the planet.

3.4.3 Factors Inhibiting Convection

The simple expectations offered by mixing length theory are modified, sometimes dramatically, by the following phenomena:

(i) *Rotation*: In the relevant limit of very small Rossby numbers, the convective motions must conform to the Taylor–Proudman theorem which enforces a columnar or plate-like pattern in which at least one of the characteristic length scales perpendicular to the rotation axis is much smaller than the large (planet scale) length of variation parallel to the rotation axis. It is likely (but not certain) that this requires a significantly larger superadiabaticity than mixing length theory predicts (for the same specified heat flux) but a convective velocity that is relatively unchanged (Stevenson 1979). However, there remains a major unresolved issue: Does convection in the presence of rotation excite large differential rotation (e.g., Aurnou and Olson 2001)? This issue is still beyond current computational capability because of the very low Ekman number of these flows. (In the actual planet, the viscosity is negligible but in numerical calculations it is chosen to be quite large since the flow would otherwise be imperfectly resolved by the numerical grid that is used.)

(ii) *Magnetic field*: In an electrical conductor, fluid motions modify the field to the extent that there is flow across field lines. The resulting induced electrical current together with the field leads to a Lorentz force whose influence on the motion can be large. In dynamos, numerical and theoretical analysis suggests that the Lorentz force, Coriolis force and buoyancy force are all comparable. The highly anisotropic nature of the rotation-dominated convection is then reduced and the convection requires less superadiabaticity than in the absence of the field. This so-called MAC state (cf. Hide and Stannard 1976, Jones 2000) leads to a different scaling of convective velocity on heat flux. If ΔT is the temperature anomaly ($\sim$ superadiabatic excess over a scale height) then the buoyancy force $g\delta\Delta T/T \sim 2\omega v_{conv}$ (the Coriolis force), where ω is the planetary angular velocity. Together with $F \sim \rho c_P \Delta T v_{conv}$ this leads to

$$v_{conv} \sim \left(\frac{g\delta F}{\rho c_P T \omega}\right)^{1/2} \tag{3.8}$$

which predicts motions of order 0.1–1 $\mathrm{cm\,s^{-1}}$ and fractional superadiabaticities of order 10^{-6} or less. In this regime where both rotation and magnetic field are important, the convective motions are one to two orders of magnitude smaller than mixing length theory predicts and compatible with the previously mentioned constraints on magnetic secular variation (Russell *et al.* 2001). We discuss the dynamo and its relation to convection further in 3.5.3.

(iii) *Compositional gradients*: The presence of compositional gradients ($\nabla_\mu \equiv d\ln\mu/d\ln P > 0$, where μ is the mean molecular weight) can lead to the inhibition of convection. The problem becomes complex because this gradient is *a priori* unknown: on one hand, convection tends to homogenize layers, leading to $\nabla_\mu \to 0$; on the other hand, sharp, diffusive interfaces can form for which $\nabla_\mu \to \infty$. This is indeed observed in the Earth oceans, where salt and heat have opposite effects. Note, however, that even in the deep oceans of Earth, vertical transport and mixing is much faster than simple diffusion would predict, because of the presence of small scale but efficient double diffusive or salt finger

instabilities. These would also occur in Jupiter, in any region where there is overall stability but the tendencies of the thermal and compositional gradients are opposed (e.g., thermal stratification that overwhelms compositional instability, or where there is compositional stratification that overwhelms thermal buoyancy).

(iv) *Condensation*: Phase changes of minor species, such as water can strongly modify convection. First, the latent heat released favors updrafts, as observed in Earth's cumulus clouds. In Jupiter's atmosphere, this leads to convective updrafts of tens of m/s. However, in hydrogen–helium atmospheres, another effect can be potentially important: in this case, because any condensing species is heavier than the surrounding environment, condensation tends to yield a stable compositional gradient ($\nabla_\mu > 0$)[‡]. Guillot (1995) shows that convection is locally inhibited when the abundance of the condensing species is larger than a certain critical value. This value is of the order of 5, 15 and 40 times the solar values for H_2O, CH_4 and NH_3, respectively. The temperature profiles of Uranus and Neptune retrieved from radio occultation of *Voyager 2* indeed show a strong superadiabaticity in the region of methane condensation, implying that convection is probably inhibited by this mechanism.

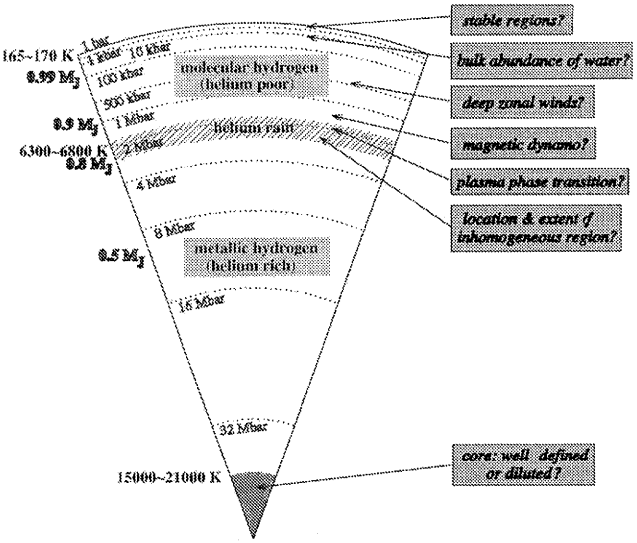

Figure 3.5. A schematic view of Jupiter's interior, together with some of the most important unanswered questions.

3.5 INTERNAL STRUCTURE

3.5.1 The Three-Layer Model

A division of Jupiter's interior into a minimum of three layers is a natural consequence of the previously discussed observational facts and theoretical inferences. These regions are: (i) a helium-poor molecular hydrogen envelope which includes the atmosphere; (ii) deeper, a helium-rich metallic hydrogen envelope; (iii) a central dense core of uncertain composition. The necessity of the helium-poor and helium-rich regions arises from the low atmospheric helium abundance and its explanation by a phase separation of helium into metallic hydrogen. The presence of a dense core is generally required to fit the gravitational moments. Because the planet is mostly convective, the helium-poor and helium-rich regions should be relatively homogeneous in terms of composition. The structure of the core itself is unknown.

This division into three regions is a good working hypothesis but it should be stressed that Jupiter may be more complex, as indicated by the questions raised in Figure 3.5. In order of significance, the first uncertainty is on the location and extent of the inhomogeneous region in which helium demixing occurs. The actual representation assumes that this region is narrow, and occurs in the low-pressure metallic hydrogen (see Section 3.3.3). It is possible that helium separates from hydrogen at larger pressures and/or on a wider pressure interval, hence requiring more complex models which are presently not available. The second unknown is the existence of a first order phase transition between molecular and metallic hydrogen (the PPT). The equilibrium of the chemical potential would then inevitably yield a different chemical composition in the two phases. This is taken into account in the three layer framework only if the helium phase separation region occurs close to the PPT. If not, another layer (between the PPT and the helium demixing zone) would have to be added to the models. Thirdly, the structure of the central core is unknown. If it is diluted, its mass would tend to be underestimated, part of it being added to the metallic region. Finally, the possible existence of stable regions at low pressures (either because of water condensation or because of a radiative zone at kbar levels) would affect mostly the temperatures at deeper levels.

In the framework of the three-layer model, one is conveniently left with only three main parameters to seek: The mass of the core, $M_{\rm core}$, and the mass mixing ratio of heavy elements in the molecular and metallic envelopes, $Z_{\rm mol}$ and $Z_{\rm met}$, respectively. (The helium mixing ratio in the molecular envelope is set equal to the atmospheric value; that in the metallic region is constrained by the fact that the total helium/hydrogen ratio should be equal to the protosolar value.) Although this is clearly a simplification of the problem, the extent of the ensemble of solutions found within this framework appears to be a useful representation of the possible structure of Jupiter's interior. This is due to the fact that because we are interested in globally averaged quantities, significant departures from the results are possible only through very different initial hypothesis on the qualitative structure of the planet.

3.5.2 Constraints on Jupiter's Composition from Interior Models

Constraints on the compositions of Jupiter and also Saturn can be obtained from numerical models solving the differential equations of hydrostatic equilibrium of a rotating fluid object. The system of equations is very similar to that describing stellar structure (e.g., Kippenhahn and Weigert 1994; for its application to giant planets see DeMarcus 1958,

‡ This is unlike the Earth's atmosphere in which the condensing molecule, water ($\mu = 18$), is lighter than air ($\mu = 29$).

Stevenson and Salpeter 1976, Zharkov and Trubitsyn 1978, Hubbard 1984; for the description of a numerical method Guillot and Morel 1995; for the extension to extrasolar giant planets and brown dwarfs Saumon *et al.* 1996, Guillot 1999b, Burrows *et al.* 2001).

The interiors of Jupiter and Saturn share many similarities. While focussing this review on Jupiter, we will also mention Saturn when results obtained for this planet can shed light on Jupiter's internal structure.

A relatively large number of models of the two giant planets have been calculated since the pioneering work of Jeffreys (1924). We will not attempt to review them exhaustively (see Hubbard and Smoluchovski 1973, Stevenson 1982b, Zharkov 1986 for reviews with a historical perspective). Focussing instead on the models calculated in the past twelve years, it is interesting to notice a relative convergence of results: Hubbard and Marley (1989) allowed the density profile to vary continuously in the molecular/metallic hydrogen transition region and found cores of the order of 8 to 14 $M_\oplus$ for Jupiter, and 9 to 20 $M_\oplus$ for Saturn, depending on the interpolation profiles between molecular and metallic hydrogen (where $M_\oplus$ is the mass of the Earth). The total masses of heavy elements that can be inferred from that work is about 30 $M_\oplus$ and 20–30 $M_\oplus$ for Jupiter and Saturn, respectively.

In the beginning of the 90s, a new astrophysical EOS for high-pressure hydrogen and helium became available (Saumon *et al.* 1995), and has been used in all interior models of Jupiter calculated since then. With that EOS, Chabrier *et al.* (1992) found core masses of 4 to 8 $M_\oplus$ and 1 to 20 $M_\oplus$, and total masses of heavy elements of 10 to 16 $M_\oplus$ and 24 to 30 $M_\oplus$ for Jupiter and Saturn, respectively. Guillot *et al.* (1994a,b) studied the effect of a radiative region at the kbar level, and obtained similar results, but with a bigger core mass (by 1–2 $M_\oplus$) and a smaller total amount of heavy elements (by ~10–20%).

In 1995, after a long journey, the *Galileo* probe successfully measured the composition and structure of Jupiter's atmosphere. The new value for the helium mass mixing ratio prompted a reexamination of previous models: because the new value of Y was higher than the *Voyager* measurement, the models matching the gravitational moments would necessarily yield a smaller quantity of heavy elements in the molecular region. Here, we will focus on results obtained since then by extensive numerical calculation in which uncertainties on observations (e.g., gravitational moments) and data (e.g., EOSs) are taken into account (Guillot, Gautier and Hubbard 1997, Guillot 1999a). These models are specifically calculated in the three-layer framework.

Before discussing these results, it is interesting to examine an alternative approach by Zharkov and Gudkova (1991) and Gudkova and Zharkov (1999). These authors calculated Jupiter's and Saturn's structure assuming a five layer structure consisting of a helium-poor external molecular region, a helium-rich internal region, a metallic region, and a two-layer helium and ice/rock core. This division is *ad hoc* and it is difficult to imagine formation and/or high-pressure processes that would have led to this particular structure. However, it is instructive to examine their results: ice/rock core masses 5 $M_\oplus$ for Jupiter and 7 $M_\oplus$ for Saturn, these planets containing about 50 $M_\oplus$ and 25 $M_\oplus$ of heavy elements, respectively (Zharkov and Gudkova 1991). With the *Galileo* data and the Saumon *et al.* (1995) EOS, Gudkova and Zharkov (1999) found generally smaller quantities (about 3 $M_\oplus$ for Jupiter's core, and ~24 $M_\oplus$ for the total mass of heavy elements). Even if the resulting global structure for Jupiter is extremely different, their results more or less agree with those presented below.

The interior three-layer models of Jupiter from Guillot *et al.* (1997) and Guillot (1999a) matching all available observations are shown in Figure 3.6. Hundreds of models have been calculated, but the solution is represented as a filled area instead of dots for an easier interpretation of the figure. A striking result obtained from Jupiter's modeling is the large uncertainty due to our relatively poor knowledge of the behavior of hydrogen at Mbar pressures. As a consequence, two kinds of solutions are found assuming (i) the Saumon–Chabrier PPT EOS, or (ii) the one that is smoothly interpolated between the molecular and the metallic fluids. The uncertainties in the solutions are *not* due to the qualitative difference at the molecular/metallic transition but instead by the quantitatively different density profiles, as seen in Figure 3.3. Any solution between the two regions in Figure 3.6 would be valid, provided the "true" EOS for hydrogen lies between the PPT and interpolated EOSs.

More quantitatively, Figure 3.6 shows that an upper limit to Jupiter's core mass is rather small, i.e., about 10 $M_\oplus$ only. This is significantly smaller than found ~20 years ago, the main difference being due to an (hopefully) improved EOS. The lower limit on the core mass is found to be zero: in this case, Jupiter could have no core, or a very small one. This corresponds however to rather extreme models, assuming a hydrogen EOS close to the interpolated one, and a large J_4 value. The lower panel of Figure 3.6 also indicates that this corresponds to a planet that is enhanced in heavy elements by 4 to 6 times over the solar value (assuming $Z_{\rm mol} = Z_{\rm met}$, a consequence of the presence of no physical discontinuity of the EOS). Generally, it is found that Jupiter's molecular region is enriched in heavy elements by 1.5 to 6.5 times the solar value, in agreement with the observations that indicate a ~3 times solar enrichment for C, N, S.

The results obtained with the PPT EOS indicate that if this EOS is valid, Jupiter would contain less heavy elements (10 to 20 $M_\oplus$) than Saturn (20 to 30 $M_\oplus$), which is unlikely. It appears that therefore Jupiter's total mass of heavy elements should be in the high end of the [10,42] $M_\oplus$ range. Note that this does not necessarily imply that the mass of the core is extremely small because it could be diluted into the bottom of the metallic envelope. Also, the uncertainty of the EOSs at pressures of tens of Mbars is difficult to estimate and could be larger than assumed here.

It is also interesting to notice that in that case, Jupiter's molecular region could be consistent with a global enrichment in heavy elements of three times the solar value, and a larger abundance of heavy elements in the metallic envelope. Globally, a three times solar enrichment of heavy elements uniformly distributed over Jupiter's envelope corresponds to a total mass of 18 $M_\oplus$. However, it has been proposed (Gautier *et al.* 2001) that the heavy elements brought to Jupiter do not necessarily need to have solar abundances, and that water could be significantly enriched. In this case, because oxygen is the third most abundant element in the universe, one can derive a useful (but high) upper limit to

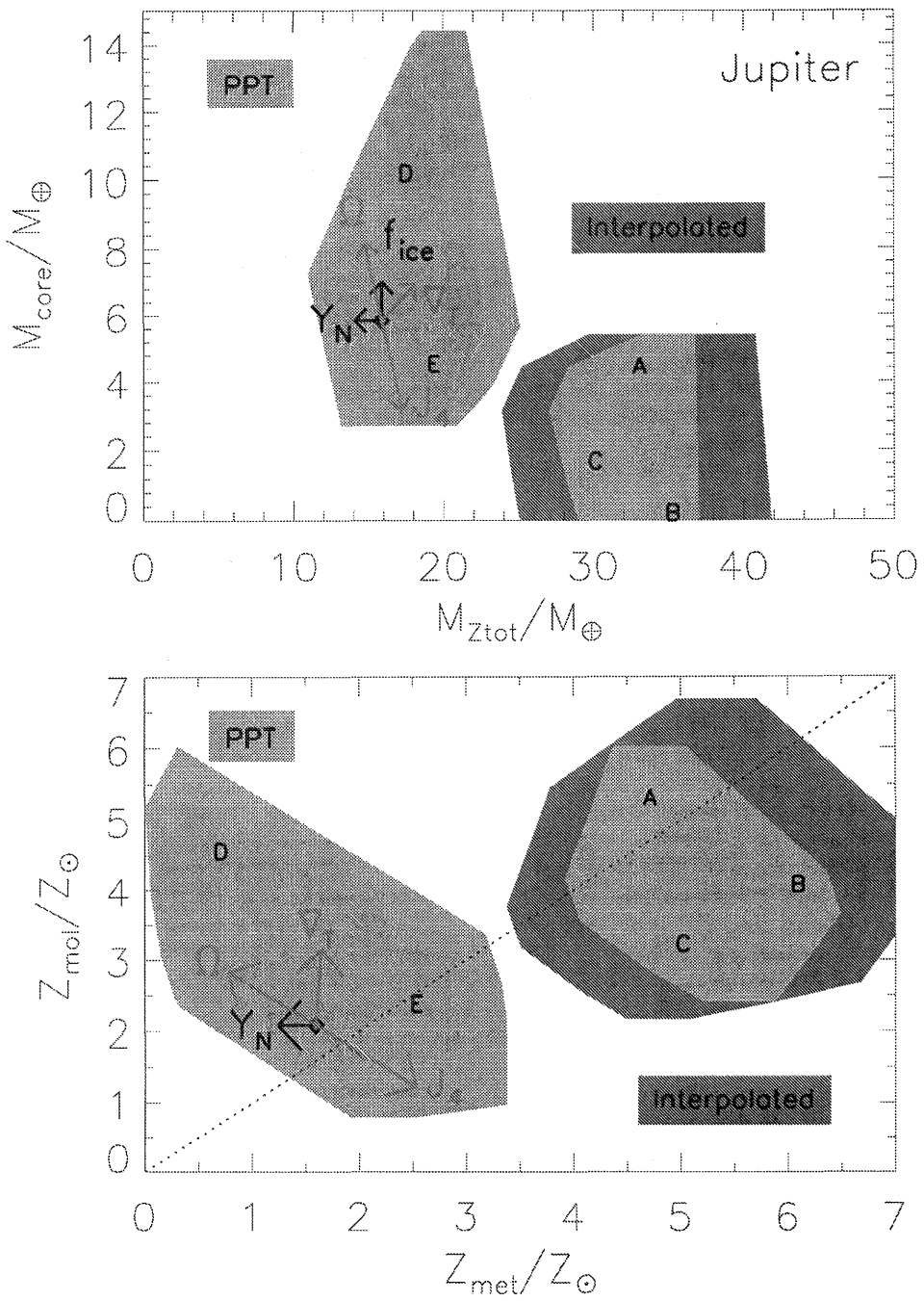

Figure 3.6. Constraints on Jupiter's interior structure. The upper panel shows values of the core mass ($M_{\rm core}$) and total mass of heavy elements ($M_{Z\rm tot}$) of models matching all available observational constraints. The lower panel shows the mass mixing ratio of heavy elements of the molecular ($Z_{\rm mol}$) and metallic ($Z_{\rm met}$) regions, in solar units ($Z_\odot = 0.0192$). The two different regions correspond to different EOSs for hydrogen (see text). Arrows indicate the direction and magnitude of the assumed uncertainties, if J_4 or $Y_{\rm proto}$ are increased by 1σ, rotation is assumed to be solid ("Ω"), the core is assumed to be composed of ices only ("$f_{\rm ice}$") and if Jupiter's interior becomes fully adiabatic ("∇_T"). The dashed line in the lower panel indicates a homogeneous abundance of heavy elements ($Z_{\rm mol} = Z_{\rm met}$). The letters A to E label sample models (see Table 3.5). Model F is indicated by a diamond. [Adapted from Guillot 1999a.]

Table 3.5. Sample models of Jupiter's interior.

Model	H EOS	Radiative zone?	T(1bar) [K]	$M_{\rm core}$ [$M_\oplus$]	M_Z [$M_\oplus$]
A	Int.	no	165	4.2	33.1
B	Int.	no	170	0	35.3
C	Int.	yes	165	1.5	30.1
D	PPT	no	170	10.0	17.5
E	PPT	no	165	4.3	19.4
F	PPT	yes	165	5.8	15.9

the abundance of water in the planet: about 10 times the solar abundance.

For reference, Table 3.5 lists a few models calculated with either the interpolated or PPT hydrogen EOS, assuming a fully convective interior or including the presence of a deep (kbar) radiative zone, and assuming a 1 bar temperature of either 165 or 170 K. These models are included as ascii files in the additional material appended to this chapter.

3.5.3 Location and Nature of Magnetic Field Generation

We could test the interior models if we knew exactly what the magnetic field says about the radius below which there is sufficient conductivity to generate a dynamo. Alternatively, we could use interior models and experimental high pressure data to test our theories of dynamos and magnetic field behavior. In reality, we are in a situation where neither the interior models nor the theory of the field is so well understood that we can treat either as the basis for a good test of the other. The best we can do is assess consistency between the different considerations. There is indeed a fairly good consistency, based on four factors: The magnetic Reynolds number (which assesses whether a dynamo is possible), the spectrum of the field (which determines the outer radius of dynamo generation), the Elsasser number (which determines the expected magnitude of the field) and the observational constraint on secular variation (which limits the amount of electromagnetic shielding that occurs exterior to the dynamo region). In addition to these four consistency checks, we have the unanswered questions concerning differential rotation and large zonal flows. We also discuss this constraint, though no data are yet available to test it.

(i) The magnetic Reynolds number. Dynamo theory (Roberts and Glatzmaier 2000, Jones 2000) tells us that a dynamo is not possible except when the magnetic Reynolds number is sufficiently large:

$$R_{\rm m} = v_{\rm conv} L/\lambda \gtrsim 10 \text{ to } 100 \tag{3.9}$$

where $v_{\rm conv}$ is the convective velocity, L is some characteristic length scale ($\sim$ size of the conducting core) and λ is the magnetic diffusivity. In SI units, $\lambda = 1/(\mu_0\sigma)$ where σ is the electrical conductivity and μ_0 is the permeability of free space. If we choose $v_{\rm conv} \sim 0.1$ to $1\,{\rm cm\,s^{-1}}$, as previously discussed, and $L \sim 10^9$ cm (15% of Jupiter's radius) then the largest acceptable value for λ is $\sim 10^7\,{\rm cm^2\,s^{-1}}$. For comparison, the Earth's core magnetic diffusivity is around $10^4\,{\rm cm^2\,s^{-1}}$, and for idealized monotonic metallic hydrogen is 10^2 to $10^3\,{\rm cm^2\,s^{-1}}$ (Stevenson and Ashcroft 1974). The highest conductivity observed in the pioneering metallization experiments (Weir *et al.* 1996, Nellis *et al.* 1999) corresponds to $\lambda \sim$ few $\times\, 10^5\,{\rm cm^2\,s^{-1}}$. The implication is that the dynamo may operate out to a pressure that is even lower than the metallization pressure of those experiments, perhaps into a regime where hydrogen is best thought of as a semiconductor. In this regime, $\sigma \sim \exp(-\delta E/2kT)$ where δE is the pressure-dependent band gap in molecular hydrogen and "metallization" is interpreted as the location ($\sim$1.6 Mbar) where δE goes to zero. If the outermost dynamo generating region is at the pressure corresponding to $\lambda \sim 10^7\,{\rm cm^2\,s^{-1}}$, then this pressure is $\sim$1.3 Mbar, corresponding to a radius $\sim$85% of Jupiter's radius. This is a slightly larger radius than previous estimates, but the rapid drop-off of conductivity with radius means that it may correspond to a significantly different (and much lower) conductivity than the usual definition of Jupiter's "metallic core". The problem with this estimate is that we have no appropriate theoretical models for dynamos functioning in large conductivity gradients.

(ii) The magnetic spectrum. As discussed in 3.2.2, the downward continuation of the field to 0.8 or 0.85 of Jupiter's radius leads to a spectrum (field energy as a function of harmonic degree) that looks similar in shape (not magnitude) to the spectrum of Earth's field evaluated at the known surface of Earth's core. At this level, the spectrum is rather "flat" (i.e., not much less energy in the octupole than in the dipole). This indicates that the argument in (i) is consistent with the observed field, the interior models, and our knowledge of how dynamos operate. However, it must be emphasized that there is a fundamental difference between Earth and Jupiter: The core–mantle boundary in Earth is very precisely defined by multiple data sets because it is a profound jump in many material properties. The surface of the dynamo in Jupiter by contrast appears to be ill-defined, e.g., probably not at the location of a phase transition or material change. It is therefore unclear to what extent we should use a direct comparison between Earth and Jupiter.

(iii) The Elsasser number. Dynamo theory tells us that we should expect a field magnitude corresponding to $\Lambda \sim 1$, where Λ is called the Elsasser number and defined:

$$\Lambda = \frac{B^2}{8\pi\rho\lambda\omega} \tag{3.10}$$

(cgs units with B in Gauss). If we use the low conductivity of the outermost region of Jupiter's dynamo and allow for the likely larger toroidal field (several tens to 100 Gauss) then $\Lambda \sim 1$ is satisfied.

(iv) Secular variations. It is also necessary that the low but non-zero conductivity outside the dynamo allow outward penetration of any observed time variation of the field. (In geophysics, this is directly analogous to the constraint people place on the conductivity of the lower mantle by analyzing geomagnetic "jerks".) If the outer edge of dynamo action is placed at $\sim$0.85 Jupiter radius, then Liu and Stevenson (in preparation, 2003) find that there is not much electromagnetic attenuation of variations with characteristic times similar to Earth or longer, consistent with the upper bound on observed secular variation (Russell *et al.* 2001). However, if the dynamo ceases at a much higher

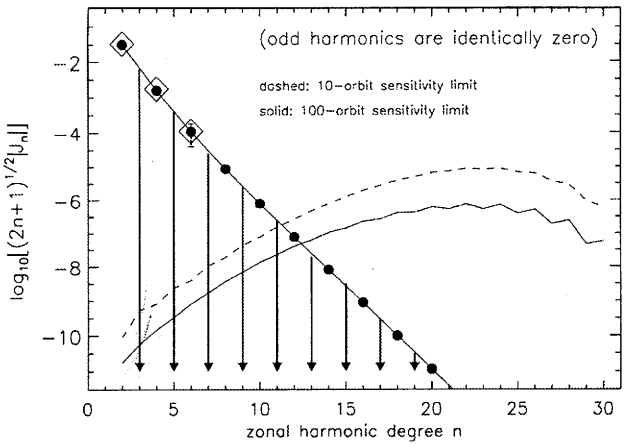

Figure 3.7. Predicted spectrum of Jupiter zonal harmonics for solid-body rotation in all layers contributing to the external gravitational potential.

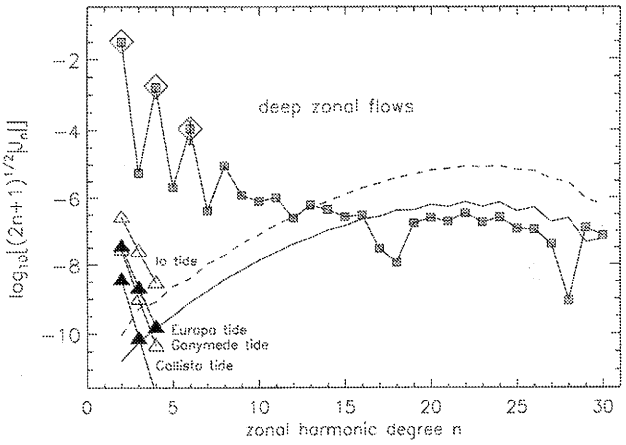

Figure 3.8. Estimated spectrum of Jupiter zonal harmonics for cylindrical rotation in all layers contributing to the external gravitational potential. Equivalent tidal response to Galilean satellites is also shown.

conductivity, then the external field would be forced to have much less time variation than Earth's field.

(v) Coupling to the zonal flow. Last but not least, we should ask about the coupling of large zonal winds to the field. For flows like those observed in the atmosphere ($\sim 10^4\,\mathrm{cm\,s^{-1}}$), one could get a magnetic Reynold's number exceeding unity even for a conductivity that is six orders of magnitude less than that usually associated with a metal (e.g., a conductivity like ocean water on Earth). This could potentially happen as far out as 90–95% of Jupiter's radius (Kirk and Stevenson 1987). Persistence of such large flows, even in a low conductivity region, would create large but not directly observable toroidal fields that would act back on the flow, reducing its strength or creating torsional oscillations (Moffatt 1978). This is poorly understood, but it suggests that there should be a connection between the structure of the magnetic field and the postulated gravity signature of differential rotation, discussed in 3.2.1. This is a challenge for future exploration.

3.5.4 Relationship to External Gravity Field

Accurate measurement of Jupiter's external gravitational potential to very high degree and order would provide data about interior structure at a level of detail well beyond that currently available. The measurements that could be made with a low-periapse orbiter, optimized to measure subtle gravitational anomalies ($\sim$1 mgal), could potentially answer a number of important questions, such as the depth of the large-scale zonal flows and the mass of a possible high-density core.

If there were no interior dynamics in Jupiter and the planet conformed to hydrostatic equilibrium in the presence of global solid-body rotation at the rotation rate of the magnetic field, the external gravitational potential would have a simple form. All odd gravitational harmonic coefficients J_3, J_5, J_7, etc. would be identically zero by symmetry. The coefficient J_2 would be directly excited by the quadrupole component of the rotational potential. All higher finite gravity coefficients are not directly excited by the solid-body rotational potential, but instead result from the planet's nonlinear response to that potential. In this case, the zonal harmonic spectrum takes the form of a geometric progression with alternating signs:

$$J_{2n+2} \sim -J_2 J_{2n} \tag{3.11}$$

Figure 3.7 shows such a zonal-harmonic spectrum for Jupiter (Hubbard 1999). The figure shows the predicted absolute values of zonal harmonics out to degree 20, calculated for a simple polytropic equation of state. The open diamonds show the available observed values for Jupiter (on this plot, an error bar is only discernable for J_6). Also shown are estimated sensitivity limits for detection of the J_n with a low-periapse orbiter (J. D. Anderson and E. Lau, private communication, 2001).

The observed zonal flows on Jupiter persist to an as-yet unknown depth. Schubert and Zhang (2000) have considered possible convection modes in giant planets, and they predict that for planets such as Jupiter, intrinsic heat flow will cause large-scale convective rolls parallel to the rotation axis to be established. The zonal flows in the observable atmosphere could thus be the surface expression of such rolls, as was initially suggested by Busse (1976). Although such convective rolls may not penetrate far into the liquid metallic-hydrogen interior at depths below ~ 8000 km due to MHD stresses, they may persist deep enough to involve significant mass, even at high latitudes.

Hubbard (1999) carried out an analysis of the implications for the high-order Jupiter gravity potential if observed atmospheric zonal flows are mapped on to concentric cylinders within the jovian interior. The steady-state structure of the interior is then given by the two-dimensional solution to the steady-state inviscid fluid equation,

$$\mathbf{v} \cdot \nabla \mathbf{v} = -\frac{1}{\rho}\nabla P + \nabla V \tag{3.12}$$

where V is the gravitational potential. Here the velocity field $\mathbf{v}$ is assumed to be time-independent and strictly zonal. Since the actual zonal flow pattern in Jupiter is not exactly north–south symmetric, rotation on cylinders cannot be consistently applied to both hemispheres simultaneously. Hubbard (1999) carries out separate solutions for Jupiter's

northern and southern hemispheres. Figure 3.8 shows a guess for the predicted harmonic spectrum for Jupiter, obtained by fitting a global gravitational potential to the northern and southern potentials simultaneously. This figure does not "predict" the magnitude of the odd zonal harmonics, such a calculation would require a detailed solution of Eq. (3.1) with north–south variation of the zonal rotation rates and baroclinic temperature profiles. However, the figure does suggest that low-order odd harmonics may be eventually detectable from a spacecraft with moderately improved sensitivity to the jovian gravity field, perhaps even with a single orbit.

According to Hubbard's (1999) calculations, if Jupiter's zonal flows persist to a depth of about 1000 km below the cloud layers, i.e., to pressures exceeding ~10 kbar, they will involve enough mass to produce gravity anomalies detectable by a low-periapse orbiter. Figure 3.9 shows a diagram illustrating the correlation between gravity anomalies and possible jovian "topography". The topography, actually the shape of isobars under the influence of zonal rotation, is shown exaggerated by about a factor of 1000. The vectors to the right of the figure show gravity anomalies calculated with respect to a planet rotating as a solid body. The maximum values of these gravity anomalies are about 30 mgal. As can be seen, the rapid zonal rotation at low latitudes causes a low-latitude height increase of the isobars, yielding extra gravity. However, the reference solid-body rotation gravity field is not observationally accessible. Instead, one will need to reference to a "smooth" gravity field, such as one generated by means of the lower zonal harmonics, say out to J_{10}. The vectors on the left-hand side of Fig. 3.9 show such anomalies, this time with a maximum amplitude ~1 mgal.

Although the dynamics-excited components of Jupiter's gravity field will be very informative about the depth of penetration of zonal flows, they are a noise source for attempts to infer the mass of a possible dense core by combining gravity data with high-pressure equations of state (Guillot, Gautier, and Hubbard 1997). An independent measurement of Jupiter's response to a perturbation field would help to remove such ambiguity. The tidal response of Jupiter to the gravitational perturbations from the Galilean satellites appears to be measurable by a low-periapse orbiter, and may provide such constraints. Figure 3.8 shows the equivalent components of Jupiter's gravity potential (expressed as zonal-harmonic coefficients) in response to the tidal perturbations of the four Galilean satellites. These components were calculated for a simple polytropic equation of state, using an approach similar to that of Gavrilov and Zharkov (1977). Although Jupiter's tidal response is ~5 to 6 orders of magnitude smaller than its response to rotation, the tidal response potential has a different spatial dependence than the rotation response potential, and, using multiple orbits, could be synchronously detected. Importantly, Jupiter tides represent a linear response to a well-characterized perturbation. Because they are time-dependent, the possibility of resonance with free-oscillation modes must be investigated. Their detection from a Jupiter orbiter would open up rich possibilities for detecting interior structure, including a dense core.

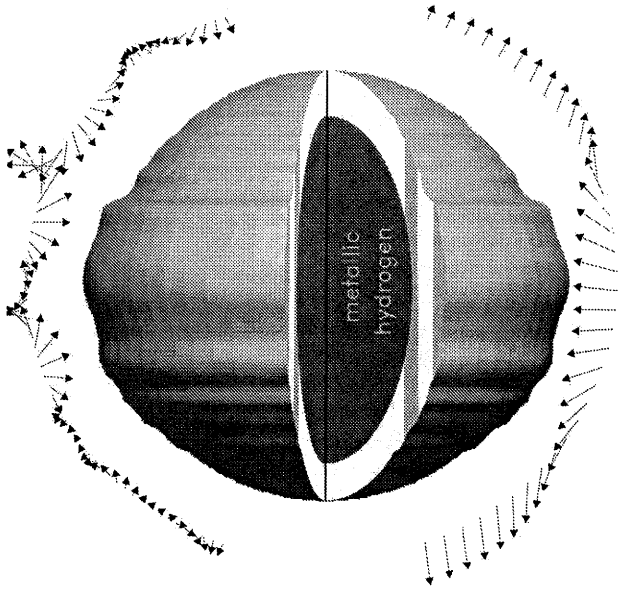

Figure 3.9. Schematic figure showing possible correlation between Jupiter "topography" produced by cylindrical zonal flows and gravity anomalies (arrows). The vectors to the right represent gravity anomalies calculated with respect to a planet rotating as a solid body. The vectors to the left represent gravity anomalies with respect to a "smooth" gravity field (calculated only from the first few gravitational moments) (see text).

3.6 EVOLUTION

3.6.1 Jupiter's Contraction

Another constraint to the problem of Jupiter's interior comes from the age of the planet as inferred from that of the solar system itself (4.55 Gyr). However, that constraint is difficult to use because it requires a good knowledge of Jupiter's atmosphere and interior not only presently but in the past as well. Modern evolution models calculated assuming a homogeneous structure (i.e., neglecting the presence of a hydrogen–helium phase separation) predict cooling times of 4.7 to 5.1 Gyr (Saumon *et al.* 1992, Guillot *et al.* 1995, Guillot 1999a). In the absence of alkali metals the presence of a radiative zone leads to a faster loss of the internal entropy of the planet and can lead to a minimum age of 3.6 Gyr. However, as discussed previously, this fast cooling is unlikely because alkali metals are expected to be present in Jupiter's atmosphere. Jupiter's models appear therefore to be cooling too slowly.

The problem is even more acute when one considers the phase separation of helium. In that case the falling of helium-rich droplets provides an additional source of energy which slows the cooling of the planet by several hundreds of millions of years (Hubbard *et al.* 1999, Guillot 1999a).

Several solutions around that problem exist. A first one is the fact that the atmospheric boundary condition still used in these evolution models is extremely coarse: basically, it is fitted to the planet's present 1 bar temperature and extrapolated to higher luminosities and atmospheric temperature using a simple relation between atmospheric temperature, effective temperature and gravity (Hubbard 1977, see

also Saumon *et al.* 1996). This is expected to introduce an uncertainty on the calculation of about 10%. Another possible factor is the fact that Jupiter was not necessarily formed from an initially infinitely extended, isotropic gas cloud. In the core-accretion formation scenario, the planet can have an extended phase of several Myr in which its mass is of order 20 $M_\oplus$. In the extreme case that this protoplanetary core is supposed to lose its entropy efficiently during that period, the subsequent evolution to Jupiter's present luminosity and radius is hastened by as much as 500 Myr. Even in the case of the gravitational collapse, the formation of an accretion disk can slow the accretion on to the central planet, allowing it to lose its entropy more efficiently than is assumed for isotropic contraction (radiation can escape freely in all directions except in the plane of rotation of the disk). Another possible explanation would be the presence of a compositional gradient deep within the planet. This can arise through the accretion but incomplete mixing of large planetesimals (up to ~Earth mass in size). In this situation, a significant portion of the planet's heat reservoir is unavailable for the total luminosity. The time required to cool to the present observed temperature is then reduced. A scenario like this has been proposed for Uranus and Neptune (Podolak *et al.* 1991, Hubbard *et al.* 1995) where there is a much more striking discrepancy between the observed heat flow and the predictions of a fully adiabatic cooling model. Finally, a perhaps even more promising explanation is that Jupiter may have formed from an initially more massive dense core and is progressively eroding it (Section 3.6.3). The massive core would have yielded an initially high intrinsic luminosity, and more energy would thus have been lost from the planet in, say, the first few millions of years. The erosion would then imply a transformation of internal energy into gravitational energy, thereby further quickening its cooling.

Figure 3.10 shows the expected variation in radius of a fully-formed Jupiter as a function of time. A first, important fact is that the planet's radius has decreased over time only by a modest factor. The evolution curve is reasonably well understood for the period that extends from about 10 Myr after Jupiter's formation onward. However, before that epoch, several factors prevent an accurate representation of the planet's evolution. As inferred from observations of young stars, it is expected that the protosolar nebula was present for about 10 Myr (this precise value being itself quite uncertain). Jupiter could then have accreted enough material from the nebula during that time to alter its evolution. Alternatively, it could have led to the end of the nebula phase by accreting most of its gas rapidly. Depending on the duration of the formation phase, Jupiter's inner regions could have had the time to cool or not, affecting the planet's energy budget. More detailed studies of that problem would require modeling the formation of a planet with a circumplanetary disk, which itself led to the formation of the regular moons.

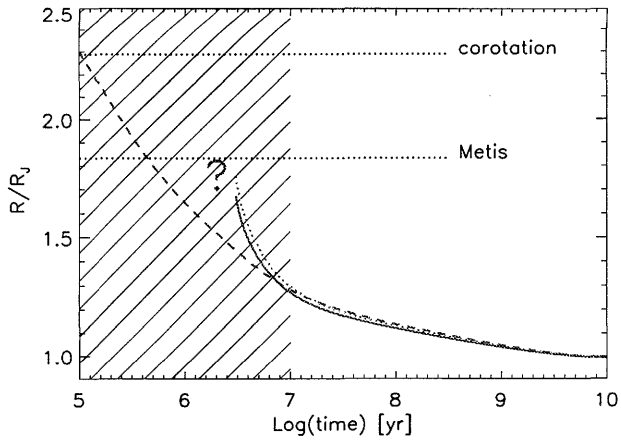

Figure 3.10. Evolution of the radius (corresponding to the 10 bar level) of a 318 $M_\oplus$ Jupiter. The dashed line corresponds to an idealized scenario in which the planet is assumed to have formed at $t = 0$ with an arbitrarily high initial radius. In the second case (solid line), an inner ~30 $M_\oplus$ is assumed to formed and cooled in 3 Myr, epoch at which the planet suddenly accreted most of its present gaseous envelope. The dotted line indicates in this case the locus of the 100 mbar radius level. As indicated by the hashed region, the inital evolution of Jupiter is expected to have occurred when the protosolar nebula was still present. The present positions of the corotation radius and semi-major axis of Metis, Jupiter's innermost moon are indicated by dotted horizontal lines.

3.6.2 On the Origin of the Heavy Element Enrichment

Jupiter and Saturn both contain a significant mass of heavy elements. Were these elements acquired early during the first phases of formation of the planets or later by impacts similar to the Shoemaker–Levy 9 event? This question is relatively new, because it is only since the in situ measurements by the *Galileo* probe that it has been proven that Jupiter's atmosphere is enriched over the solar value in several elements.

A first possible explanation may be that Jupiter and Saturn, after their formation, cleared the nebula of its planetesimals and acquired a fraction of them. Dynamical simulations (Guillot and Gladman 2001, Hahn and Malhotra 1999) show however that as soon as Jupiter grows to its present mass, the accretion efficiency of all giant planets becomes small. Quantitatively, if they were suddenly plunged into a 100 $M_\oplus$ disk of planetesimals distributed between 4 and 35 AU, Jupiter and Saturn (with their present masses, radii and orbital parameters) would accrete about 4.4 $M_\oplus$ and 0.9 $M_\oplus$, respectively, the rest of the planetesimals being ejected by Jupiter or sent to the Oort cloud (Guillot and Gladman 2001). This result is for a disk surface density $\sigma \propto r^{-3/2}$ (r being the heliocentric distance), but changing that distribution has only modest consequences. The result should also hold for the same fully-formed planets 4.5 Gyr ago, because of the modest increase in their radii (Figure 3.10). For comparison, Pollack *et al.* (1996) require a disk mass of 220 $M_\oplus$ in solids (and its complement in gas) between 4 and 35 AU to form Jupiter, Saturn and Uranus. Given the fact that most of the mass that is initially close to a giant planet and has the largest impact probability is used to form a core during the runaway growth phase, it appears that it is difficult to account for the observed atmospheric enrichment of Jupiter and Saturn in the framework of a late accretion of planetesimals scenario (after Jupiter's mass increased to ~300 $M_\oplus$).

An alternative scenario could be that Jupiter and

Saturn formed rapidly in a still massive nebula (Boss 2000 and references therein). However, the problem may be even more difficult because a mechanism then needs to be found to prevent gas accretion by the giant planets, while allowing the capture of solid bodies.

A more plausible explanation is hence that the giant planets acquired their heavy elements through the rapid growth of their cores (the runaway growth phase–see Safronov 1972, Lissauer 1993), and in a phase in which they had grown to about $\sim$20 $M_\oplus$ and in which they were in quasi-static equilibrium with the surrounding nebula (Pollack *et al.* 1996). In that later phase, the accretion efficiency is increased significantly (Guillot and Gladman 2001) due (i) to a smaller probability of ejection of planetesimals out of the solar system (Jupiter being much less massive than it is today) and (ii) to a larger effective capture radius by the very extended gaseous envelopes (e.g., Podolak *et al.* 1988).

Because the planetesimals are almost always dissolved very close to the central regions (Podolak *et al.* 1988, Pollack *et al.* 1996), the rapid capture of the gas of the nebula is expected to create a giant planet consisting mostly of a massive core and a low-metallicity gaseous envelope. This scenario implies that part of this primordial core had to be eroded to enrich the gaseous envelope in heavy elements.

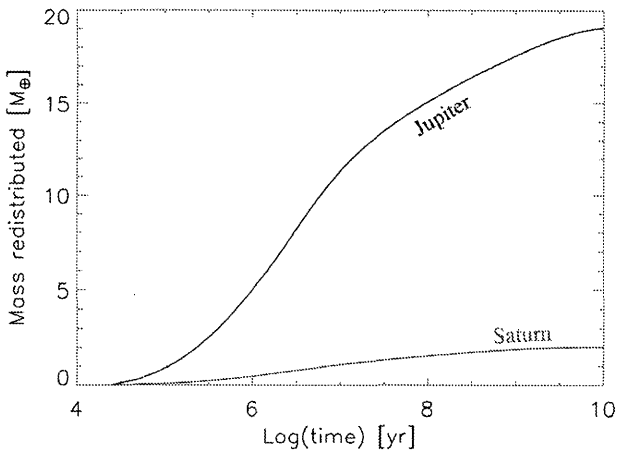

Figure 3.11. Mass of heavy elements initially embedded in a central core and progressively redistributed, according to a speculative scenario in which 10% ($\chi = 0.1$) of the intrinsic energy flux in the first pressure scale height is used to mix the heavy elements upward [see Eq. (3.14)]. Jupiter and Saturn were assumed to consist of a 30 $M_\oplus$ core and a hydrogen–helium envelope. The decrease of the core mass in time and the non-zero compressibility of core material were neglected in the calculation of ϖ.

3.6.3 Core Erosion

To first order, the redistribution of a small core of mass $\Delta m_{\rm core}$ in a planet of total mass M and radius R "costs" in terms of energy:

$$\Delta E_{\rm grav} = -\varpi \frac{GM}{R} \Delta m_{\rm core} \tag{3.13}$$

where ϖ is a factor of order unity, which is equal to 3/10 in the limit of a very small core of finite density, and a fully incompressible planet (a sufficient approximation for our purposes). The erosion of the core can be thought to proceed through the penetration of downward convective plumes. In that case, the erosion mass flux is:

$$\dot{m}_{\rm core}(t) = -\frac{\chi}{\varpi} \frac{RL_1(t)}{GM} \tag{3.14}$$

where $L_1(t)$ is the planet's intrinsic luminosity in the first convective cell (after one pressure scale height), and χ is an efficiency factor. As discussed by Stevenson (1982c), the erosion is limited by diffusion processes at the core/envelope interface, and one can expect that $\chi \approx (D/K)^{1/2}$ where D and K are the molecular and thermal diffusivity, respectively. For metallic hydrogen, one expects $D \sim 10^{-3} - 10^{-4}\,{\rm cm^2\,s^{-1}}$ and $K \sim 10^{-1}\,{\rm cm^2\,s^{-1}}$ (Stevenson and Salpeter 1977a, Stevenson 1982c), implying, within an order of magnitude, $\chi \sim 0.1$.

Figure 3.11 shows the evolution of $\int_0^t \dot{m}_{\rm core} {\rm d}t$ for Jupiter and Saturn. In the figure, the $t = 0$ origin corresponds to the time at which the planets accrete their gaseous envelopes. In the simulations, the two planets were assumed to possess a 30 $M_\oplus$ core. The value of ϖ was calculated for an incompressible planet (both for the core and the envelope). The parameter χ was arbitrarily set to 0.1. Apart from the quantitative results which are quite uncertain (both because of uncertainties of χ and of our assumption of downward overshoot of convective plumes in the first pressure scale height which represent a significant $\sim$10% fraction of the planet), it is interesting to notice that the redistribution of the core mass would have been much more pronounced in Jupiter than in Saturn. This is in agreement with interior models that generally predict that Jupiter has a smaller core than Saturn (e.g., Guillot 1999a). With simple hypotheses (quasi-homogeneous planets and a solar C/O ratio), the observed atmospheric abundances appear to require the redistribution of $\sim$18 $M_\oplus$ in Jupiter and $\sim$4 $M_\oplus$ in Saturn. The difference between Jupiter and Saturn is more pronounced in Figure 3.11, but it may be advocated (i) that with a slightly larger χ factor, Jupiter's core may have been fully eroded and (ii) that while we have assumed ϖ of order unity, this parameter will be smaller for material with a large compressibility. A full modeling of the evolution of the cores of the two planets including consistent high-pressure equations of state would be required in order to further test this hypothesis.

The possible erosion of the cores of Jupiter and Saturn is important for formation models in the core accretion scenario. As shown by Pollack *et al.* (1996) (see also Chapter 2), the formation of a small ($\sim$10 $M_\oplus$) core requires a relatively low surface density of solids in the protosolar nebula and a consequently relatively long formation timescale ($\sim$8 Myr). However, if Jupiter's primordial core is allowed to be relatively large, this constraint is relaxed, and the planet could thus form rapidly.

3.7 FUTURE PROSPECTS

Despite numerous space missions that have flown past Jupiter, the planet has kept many of its secrets: we do not know what quantities of heavy elements it contains, we do not know if it possesses a central core, and we still have to guess how and where its magnetic field is generated. Progress concerning these key questions will be partly

addressed by better experimental results on hydrogen compression to ultra-high pressures. However, improvement in our knowledge of Jupiter's interior will eventually require three key measurements: (i) a determination of the bulk abundance of water; (ii) mapping the planet's gravity field with high accuracy and spatial resolution; (iii) mapping the planet's magnetic field with high accuracy and spatial resolution.

These measurements could be accomplished in the near future by sending a spacecraft within ~3000 km of Jupiter's cloud tops, much closer than any previous spacecraft (except the *Galileo* probe). The abundance of water at deep levels (~100 bars and more) could then be retrieved from the brightness temperature at millimeter wavelengths, the low altitude preventing confusion from synchrotron emission (Bolton *et al.* 2001). With a low-periapse orbiter, the gravity field can be mapped with very high accuracy, so that gravitational components arising from non-hydrostatic effects can be measured (Hubbard 1999). The magnetic field can be characterized at the same time in all its complexity.

In parallel, further progress in understanding Jupiter's interior will come from theoretical studies of: (i) improved equations of state and solubilities of hydrogen, helium and other elements; (ii) specific atmospheric models that account for the stellar irradiation, observed non-solar abundances of chemical elements and presence of moist convection; (iii) models of convection in the presence of rotation and magnetic fields; (iv) a description of the core/envelope interface from the point of view of fluid dynamics (including diffusion, conduction and convection in the presence of molecular weight gradients); (v) a theory of rotating fluid figures of (non-idealized) giant planets in the presence of complex internal rotation patterns. These improvements will pave the way for more realistic interior models fitting the gravitational field in all its complexity, and for detailed evolution models that can account for Jupiter's age of ~4.55 Gyr.

Jupiter's exploration must be pursued because it has far-reaching astrophysical consequences. While the *Galileo* probe has precisely measured the abundance of helium in Jupiter's atmosphere, the determination of the abundance of water in Jupiter's interior would constitute a great leap in completing the inventory of oxygen in the solar system. Oxygen being the third most abundant element in the universe, this is an important clue to understanding how our solar system was formed. Similarly, measuring Jupiter's deep winds has implications not only on the planetary structure but on meteorology in general. Jupiter also has the second most powerful magnetic dynamo in the solar system (after the Sun's), and understanding it is crucial for magnetohydrodynamics in general. Finally, Jupiter appears to be a nearby example of a new class of astronomical objects: giant planets and substellar objects (brown dwarfs). With more than a hundred members (see e.g., Mayor and Queloz 1995, Marcy *et al.* 2000 and the discoverers' web pages), this new class must be characterized by a dual approach: (i) observations of extrasolar planetary systems, for which statistically significant information can be sought and (ii) a precise exploration of the giant planets in the solar system, especially Jupiter, for which much more elaborate data can be gathered and physical processes can be studied in detail.

Acknowledgements. This work was supported in part by the Programme National de Planétologie, by an Action Concertée Incitative of the French Ministère de la Recherche, by NASA grants NAG5-7211, NAG5-7499, NAG5-10629 (Origins Program), NAG5-4214 (Planetary Astronomy), NAG5-7073, NAG5-10760 (Astrophysics Theory), NAG5-8906 (Planetary Geology and Geophysics Program), and by the US Department of Energy under contract W-7405-ENG-36.

Material appended to this chapter: 15 ascii files (representing evolution and interior models of Jupiter) are on the accompanying CD and can also be found at the following site:
ftp://ftp.obs-nice.fr/pub/guillot/jupbook/

REFERENCES

Acuña, M. H., J. E. P. Connerney, and N. F. Ness, The Z3 zonal harmonic model of Saturn's magnetic field: Analyses and implications, *J. Geophys. Res.* **88**, 8771–8778, 1983.

Aurnou, J. M. and P. L. Olson, Strong zonal winds from thermal convection in a rotating spherical shell, *Geophys. Res. Let.* **28**, 2557, 2001.

Bahcall, J. N., M. H. Pinsonneault, and G. J. Wasserburg, Solar models with helium and heavy-element diffusion, *Rev. Mod. Phys.* **67**, 781–808, 1995.

Beule, D., W. Ebeling, A. Förster, H. Juranek, S. Nagel, R. Redmer, and G. Röpke, Equation of state for hydrogen below 10 000 K: From the fluid to the plasma, *Phys. Rev. B* **59**, 14 177–14 181, 1999.

Bolton, S. J., T. Owen, D. Gautier, S. Gulkis, M. Janssen, S. Atreya, T. Guillot, J. Anderson, M. Allison, and J. Lunine, Jupiter: Atmospheric Sounding and Sensing of the Interior (JASSI), in *Forum on Innovative Approaches to Outer Planetary Exploration 2001-2020*, p. 12, 2001.

Boss, A. P., Possible rapid gas giant planet formation in the solar nebula and other protoplanetary disks, *ApJ* **536**, L101–L104, 2000.

Burrows, A., M. S. Marley, and C. M. Sharp, The near-infrared and optical spectra of methane dwarfs and brown dwarfs, *ApJ* **531**, 438–446, 2000.

Burrows, A., W. B. Hubbard, J. I. Lunine, and J. Liebert, The theory of brown dwarfs and extrasolar giant planets, *Rev. Mod. Phys.* **73**, 719–765, 2001.

Busse, F. H., A simple model of convection in the jovian atmosphere, *Icarus* **29**, 255–260, 1976.

Campbell, J. K. and S. P. Synnott, Gravity field of the jovian system from *Pioneer* and *Voyager* tracking data, *AJ* **90**, 364–372, 1985.

Celliers, P. M., G. W. Collins, L. B. da Silva, D. M. Gold, R. Cauble, R. J. Wallace, M. E. Foord, and B. A. Hammel, Shock-induced transformation of liquid deuterium into a metallic fluid, *Phys. Rev. Lett.* **84**, 5564–5567, 2000.

Chabrier, G., D. Saumon, W. B. Hubbard, and J. I. Lunine, The molecular–metallic transition of hydrogen and the structure of Jupiter and Saturn, *ApJ* **391**, 817–826, 1992.

Chau, R., A. C. Mitchell, R. W. Minich, and W. J. Nellis, Electrical conductivity of water compressed dynamically to pressures of 70–180 GPa (0.7–1.8 Mbar), *Jour. Chem. Phys.* **114**, 1361–1365, 2001.

Cohen, E. R. and B. N. Taylor, The 1986 adjustment of the fundamental physical constants, *Rev. Mod. Phys.* **59**, 1121–1148, 1987.

Collins, G. W., L. B. da Silva, P. Celliers, D. M. Gold, M. E. Foord, R. J. Wallace, A. Ng, S. V. Weber, K. S. Budil, and R. E. Cauble, Measurements of the equation of state of deu-

terium at the fluid insulator-metal transition, *Science* **281**, 1178–1181, 1998.

Collins, G. W., P. M. Celliers, L. B. da Silva, R. Cauble, D. M. Gold, M. E. Foord, N. C. Holmes, B. A. Hammel, R. J. Wallace, and A. Ng, Temperature measurements of shock compressed liquid deuterium up to 230 GPa, *Phys. Rev. Lett.* **87**, 165,504, 2001.

Connerney, J. E. P., M. H. Acuna, and N. F. Ness, *Voyager 1* assessment of Jupiter's planetary magnetic field, *J. Geophys. Res.* **87**, 3623–3627, 1982.

Conrath, B. J., R. A. Hanel, and R. E. Samuelson, Thermal structure and heat balance of the outer planets, in *Origin and Evolution of Planetary and Satellite Atmospheres*, pp. 513–538, 1989.

Da Silva, L. B., P. Celliers, G. W. Collins, K. S. Budil, N. C. Holmes, T. W. Barbee, B. A. Hammel, J. D. Kilkenny, R. J. Wallace, M. Ross, R. Cauble, A. Ng, and G. Chiu, Absolute equation of state measurements on shocked liquid deuterium up to 200 GPa (2 Mbar), *Phys. Rev. Lett.* **78**, 483–486, 1997.

Davies, M. E., V. K. Abalakin, M. Bursa, T. Lederle, J. H. Lieske, R. H. Rapp, P. K. Seidelman, A. T. Singclair, V. G. Tejfel, and Y. S. Tjuflin, Report of the IAU/IAG COSPAR working group on cartographic coordinates and rotational elements of the planets and satellites: 1985, *Celest. Mech.* **39**, 102–113, 1986.

DeMarcus, W. C., The constitution of Jupiter and Saturn, *AJ* **63**, 2, 1958.

Deming, D., M. J. Mumma, F. Espenak, D. E. Jennings, T. Kostiuk, G. Wiedemann, R. Loewenstein, and J. Piscitelli, A search for p-mode oscillations of Jupiter: Serendipitous observations of nonacoustic thermal wave structure, *ApJ* **343**, 456–467, 1989.

Dormy, E., J. P. Valet, and V. Courtillot, Numerical models of the geodynamo and observational constraints, *Geochem. Geophys. Geosystems* **1**, 62, 2000.

Fortney, J. and W. Hubbard, Phase separation in giant planets: Inhomogeneous evolution of Saturn, *Icarus* **in press**, 2003.

Galli, G., R. Q. Hood, A. U. Hazi, and F. Gygi, Ab initio simulations of compressed liquid deuterium, *Phys. Rev. B* **61**, 909–912, 2000.

Gautier, D., F. Hersant, O. Mousis, and J. I. Lunine, Erratum: Enrichments in volatiles in Jupiter: A new interpretation of the *Galileo* measurements, *ApJ* **559**, L183–L183, 2001.

Gavrilov, S. V. and V. N. Zharkov, Love numbers of the giant planets, *Icarus* **32**, 443–449, 1977.

Gierasch, P. J. and B. J. Conrath, Dynamics of the atmospheres of the outer planets: Post-*Voyager* measurement objectives, *J. Geophys. Res.* **98**, 5459–5469, 1993.

Goldreich, P. and P. Kumar, The interaction of acoustic radiation with turbulence, *ApJ* **326**, 462–478, 1988.

Goldreich, P. and S. Soter, Q in the solar system, *Icarus* **5**, 375–389, 1966.

Gudkova, T. V. and V. N. Zharkov, Models of Jupiter and Saturn after *Galileo* mission, *Plan. Space Sci.* **47**, 1201–1210, 1999.

Guillot, T., Condensation of methane ammonia and water in the inhibition of convection in giant planets, *Science* **269**, 1697, 1995.

Guillot, T., A comparison of the interiors of Jupiter and Saturn, *Plan. Space Sci.* **47**, 1183–1200, 1999a.

Guillot, T., Interior of giant planets inside and outside the solar system, *Science* **286**, 72–77, 1999b.

Guillot, T. and B. Gladman, Late planetesimal delivery and the composition of giant planets, in *Proceedings of the Disks, Planetesimals, and Planets conference*, F. Garzon, ed., pp. 475–485, 2000.

Guillot, T. and P. Morel, CEPAM: a code for modeling the interiors of giant planets., *A&AS* **109**, 109–123, 1995.

Guillot, T. and A. P. Showman, Evolution of "51 Pegasus b-like" planets, *A&A* **385**, 156–165, 2002.

Guillot, T., G. Chabrier, P. Morel, and D. Gautier, Nonadiabatic models of Jupiter and Saturn, *Icarus* **112**, 354–367, 1994a.

Guillot, T., D. Gautier, G. Chabrier, and B. Mosser, Are the giant planets fully convective?, *Icarus* **112**, 337–353, 1994b.

Guillot, T., G. Chabrier, D. Gautier, and P. Morel, Effect of radiative transport on the evolution of Jupiter and Saturn, *ApJ* **450**, 463, 1995.

Guillot, T., A. Burrows, W. B. Hubbard, J. I. Lunine, and D. Saumon, Giant planets at small orbital distances, *ApJ* **459**, L35+, 1996.

Guillot, T., D. Gautier, and W. B. Hubbard, New constraints on the composition of Jupiter from *Galileo* measurements and interior models, *Icarus* **130**, 534–539, 1997.

Hahn, J. M. and R. Malhotra, Orbital evolution of planets embedded in a planetesimal disk, *AJ* **117**, 3041–3053, 1999.

Hanel, R., B. Conrath, L. Herath, V. Kunde, and J. Pirraglia, Albedo, internal heat, and energy balance of Jupiter: Preliminary results of the *Voyager* infrared investigation, *J. Geophys. Res.* **86**, 8705–8712, 1981.

Hemley, R. J., H. K. Mao, L. W. Finger, A. P. Jephcoat, R. M. Hazen, and C. S. Zha, Equation of state of solid hydrogen and deuterium from single-crystal x-ray diffraction to 26.5 GPa, *Phys. Rev. B* **42**, 6458–6470, 1990.

Hide, R. and D. Stannard, Jupiter's magnetism: Observations and theory, in *Jupiter*, T. Gehrels (ed), University of Arizona Press, pp. 767–787, 1976.

Holmes, N. C., M. Ross, and W. J. Nellis, Temperature measurements and dissociation of shock-compressed liquid deuterium and hydrogen, *Phys. Rev. B* **52**, 15 835–15 845, 1995.

Hubbard, W. B., Thermal structure of Jupiter, *ApJ* **152**, 745–754, 1968.

Hubbard, W. B., The jovian surface condition and cooling rate, *Icarus* **30**, 305–310, 1977.

Hubbard, W. B., Effects of differential rotation on the gravitational figures of Jupiter and Saturn, *Icarus* **52**, 509–515, 1982.

Hubbard, W. B., *Planetary Interiors*, Van Nostrand Reinhold Company, New York, 1984.

Hubbard, W. B., Gravitational signature of Jupiter's deep zonal flows, *Icarus* **137**, 357–359, 1999.

Hubbard, W. B. and H. E. Dewitt, Statistical mechanics of light elements at high pressure: VII. A perturbative free energy for arbitrary mixtures of H and He, *ApJ* **290**, 388–393, 1985.

Hubbard, W. B. and M. S. Marley, Optimized Jupiter, Saturn, and Uranus interior models, *Icarus* **78**, 102–118, 1989.

Hubbard, W. B. and W. L. Slattery, Interior structure of Jupiter Theory of gravity sounding, in *Jupiter*, T. Gehrels (ed), University of Arizona Press, pp. 176–194, 1976.

Hubbard, W. B. and R. Smoluchowski, Structure of Jupiter and Saturn, *Space Sci. Rev.* **14**, 599, 1973.

Hubbard, W. B. and D. J. Stevenson, Interior structure of Saturn, in *Saturn*, T. Gehrels and M. S. Matthews (eds), University of Arizona Press, pp. 47–87, 1984.

Hubbard, W. B., M. Podolak, and D. J. Stevenson, The interior of Neptune, in *Neptune and Triton*, D. P. Cruikshank (ed), University of Arizona Press, pp. 109–138, 1995.

Hubbard, W. B., T. Guillot, M. S. Marley, A. Burrows, J. I. Lunine, and D. S. Saumon, Comparative evolution of Jupiter and Saturn, *Plan. Space Sci.* **47**, 1175–1182, 1999.

Jeffreys, H., On the internal constitution of Jupiter and Saturn, *MNRAS* **84**, 534, 1924.

Jones, C. A., Convection-driven geodynamo models, *Philos. Trans. Roy. Soc. A.* **358**, 873–897, 2000.

Kerley, G. I., Equation of state and phase diagram of dense hydrogen, *Phys. Earth Planet. Interiors* **6**, 78–82, 1972.

Kippenhahn, R. and A. Weigert, *Stellar Structure and Evolution*, Springer-Verlag, 1994.

Kirk, R. L. and D. J. Stevenson, Hydromagnetic constraints on

deep zonal flow in the giant planets, *ApJ* **316**, 836–846, 1987.

Klepeis, J. E., K. J. Schafer, T. W. Barbee, and M. Ross, Hydrogen–helium mixtures at megabar pressures: Implications for Jupiter and Saturn, *Science* **254**, 986–989, 1991.

Knudson, M. D., D. L. Hanson, J. E. Bailey, C. A. Hall, J. R. Asay, and W. W. Anderson, Equation of state measurements in liquid deuterium to 70 GPa, *Phys. Rev. Lett.* **87**, 225,501, 2001.

Landau, L. D. and E. Lifshitz, *Statistical physics*, Pergamon Press, 1969.

Lederer, S. M., M. S. Marley, B. Mosser, J. P. Maillard, N. J. Chanover, and R. F. Beebe, Albedo features and jovian seismology, *Icarus* **114**, 269–277, 1995.

Lenosky, T. J., J. D. Kress, and L. A. Collins, Molecular-dynamics modeling of the Hugoniot of shocked liquid deuterium, *Phys. Rev. B* **56**, 5164–5169, 1997.

Lenosky, T. J., S. R. Bickham, J. D. Kress, and L. A. Collins, Density-functional calculation of the Hugoniot of shocked liquid deuterium, *Phys. Rev. B* **61**, 1–4, 2000.

Lindal, G. F., G. E. Wood, G. S. Levy, J. D. Anderson, D. N. Sweetnam, H. B. Hotz, B. J. Buckles, D. P. Holmes, P. E. Doms, V. R. Eshleman, G. L. Tyler, and T. A. Croft, The atmosphere of Jupiter: An analysis of the *Voyager* radio occultation measurements, *J. Geophys. Res.* **86**, 8721–8727, 1981.

Lissauer, J. J., Planet formation, *Ann. Rev. Astron. Astrophys.* **31**, 129–174, 1993.

Low, F. J., Observations of Venus, Jupiter, and Saturn at $\lambda 20\ \mu$, *AJ* **71**, 391, 1966.

Lubow, S. H., C. A. Tout, and M. Livio, Resonant tides in close orbiting planets, *ApJ* **484**, 866, 1997.

Mahaffy, P. R., H. B. Niemann, A. Alpert, S. K. Atreya, J. Demick, T. M. Donahue, D. N. Harpold, and T. C. Owen, Noble gas abundance and isotope ratios in the atmosphere of Jupiter from the *Galileo* Probe Mass Spectrometer, *J. Geophys. Res.* **105**, 15 061–15 072, 2000.

Marcy, G. W., R. P. Butler, E. Williams, L. Bildsten, J. R. Graham, A. M. Ghez, and J. G. Jernigan, The planet around 51 Pegasi, *ApJ* **481**, 926, 1997.

Marcy, G. W., W. D. Cochran, and M. Mayor, Extrasolar planets around main-sequence stars, *Protostars and Planets IV* p. 1285, 2000.

Mayor, M. and D. Queloz, A Jupiter-mass companion to a solar-type star, *Nature* **378**, 355, 1995.

Militzer, B. and D. M. Ceperley, Path integral Monte Carlo calculation of the deuterium hugoniot, *Phys. Rev. Lett.* **85**, 1890–1893, 2000.

Militzer, B. and D. M. Ceperley, Path integral Monte Carlo simulation of the low-density hydrogen plasma, *Phys. Rev. E* **63**, 66,404, 2001.

Moffatt, H. K., *Magnetic Field Generation in Electrically Conducting Fluids*, Cambridge University Press, 1978.

Mosser, B., J. P. Maillard, and D. Mékarnia, New attempt at detecting the jovian oscillations, *Icarus* **144**, 104–113, 2000.

Mostovych, A. N., Y. Chan, T. Lehecha, A. Schmitt, and J. D. Sethian, Reflected shock experiments on the equation-of-state properties of liquid deuterium at 100–600 GPa (1–6 Mbar), *Phys. Rev. Lett.* **85**, 3870–3873, 2000.

Nellis, W. J., A. C. Mitchell, M. van Thiel, G. J. Devine, R. J. Trainor, and N. Brown, Equation of state data for molecular hydrogen and deuterium at shock pressures in the range 2–76 Gpa (20–760 kbar), *J. Chem. Phys.* **79**, 1480–1486, 1983.

Nellis, W. J., N. C. Holmes, A. C. Mitchell, G. K. Governo, M. Ross, D. A. Young, and R. J. Trainor, Shock compression of liquid helium to 56 GPa (560 kbar), *Phys. Rev. Lett.* **53**, 1248–1251, 1984.

Nellis, W. J., N. C. Holmes, A. C. Mitchell, D. C. Hamilton, and M. Nicol, Equation of state and electrical conductivity of "synthetic Uranus," a mixture of water, ammonia, and isopropanol, at shock pressure up to 200 GPa (2 Mbar), *Jour. Chem. Phys.* **107**, 9096–9100, 1997.

Nellis, W. J., S. T. Weir, and A. C. Mitchell, Minimum metallic conductivity of fluid hydrogen at 140 GPa (1.4 Mbar), *Phys. Rev. B* **59**, 3434–3449, 1999.

Niemann, H. B., S. K. Atreya, G. R. Carignan, T. M. Donahue, J. A. Haberman, D. N. Harpold, R. E. Hartle, D. M. Hunten, W. T. Kasprzak, P. R. Mahaffy, T. C. Owen, and S. H. Way, The composition of the jovian atmosphere as determined by the *Galileo* Probe Mass Spectrometer, *J. Geophys. Res.* **103**, 22 831–22 846, 1998.

Owen, T., P. Mahaffy, H. B. Niemann, S. Atreya, T. Donahue, A. Bar-Nun, and I. de Pater, A low-temperature origin for the planetesimals that formed Jupiter, *Nature* **402**, 269–270, 1999.

Peale, S. J., Origin and evolution of the natural satellites, *Ann. Rev. Astron. Astrophys.* **37**, 533–602, 1999.

Pearle, J. C. and B. J. Conrath, The albedo, effective temperature, and energy balance of Neptune, as determined from *Voyager* data, *J. Geophys. Res.* **96**, 18 921–18 930, 1991.

Pfaffenzeller, O., D. Hohl, and P. Ballone, Miscibility of hydrogen and helium under astrophysical conditions, *Phys. Rev. Lett.* **74**, 2599–2602, 1995.

Podolak, M., J. B. Pollack, and R. T. Reynolds, Interactions of planetesimals with protoplanetary atmospheres, *Icarus* **73**, 163–179, 1988.

Podolak, M., W. B. Hubbard, and D. J. Stevenson, Model of Uranus' interior and magnetic field, in *Uranus*, J. T. bergstralh, E. D. Miner and M. S. Matthews (eds), University of Arizona Press, pp. 29–61, 1991.

Pollack, J. B., O. Hubickyj, P. Bodenheimer, J. J. Lissauer, M. Podolak, and Y. Greenzweig, Formation of the giant planets by concurrent accretion of solids and gas, *Icarus* **124**, 62–85, 1996.

Roberts, P. H. and G. A. Glatzmaier, Geodynamo theory and simulations, *Rev. Mod. Phys.* **72**, 1081–1123, 2000.

Rogers, F. J., Ionization equilibrium and equation of state in strongly coupled plasmas, *Phys. Plasmas* **7**, 51–58, 2000.

Ross, M., Linear-mixing model for shock-compressed liquid deuterium, *Phys. Rev. B* **58**, 669–677, 1998.

Ross, M. and L. H. Yang, Effect of chainlike structures on shock-compressed liquid deuterium, *Phys. Rev. B* **64**, 134,210, 2001.

Roulston, M. S. and D. J. Stevenson, Prediction of neon depletion in Jupiter's atmosphere, *EOS* **76**, 343, 1995. Abstract.

Russell, C. T., Z. J. Yu, K. K. Khurana, and M. G. Kivelson, Magnetic field changes in the inner magnetosphere of Jupiter, *Adv. Space Res.* **28**, 897–902, 2001.

Safronov, V. S., *Evolution of the Protoplanetary Cloud and Formation of the Earth and Planets*, Israel Program for Scientific Translations, Jerusalem, 1972.

Salpeter, E. E., On convection and gravitational layering in Jupiter and in stars of low mass, *ApJ* **181**, L83+, 1973.

Saumon, D., W. B. Hubbard, G. Chabrier, and H. M. van Horn, The role of the molecular-metallic transition of hydrogen in the evolution of Jupiter, Saturn, and brown dwarfs, *ApJ* **391**, 827–831, 1992.

Saumon, D., G. Chabrier, and H. M. van Horn, An equation of state for low-mass stars and giant planets, *ApJS* **99**, 713, 1995.

Saumon, D., W. B. Hubbard, A. Burrows, T. Guillot, J. I. Lunine, and G. Chabrier, A theory of extrasolar giant planets, *ApJ* **460**, 993, 1996.

Saumon, D., D. J. Chabrier, G. Wagner, and X. Xie, Modeling pressure-ionization of hydrogen in the context of astrophysics, *High Pressure Res.* **16**, 331–343, 2000.

Schmider, F.-X., E. Fossat, and B. Mosser, Possible detection of jovian global oscillations, *A&A* **248**, 281–291, 1991.

Schubert, G. and K. Zhang, Dynamics of giant planet interiors, in *From Giant Planets to Cool Stars*, p. 210, 2000.

Seiff, A., D. B. Kirk, T. C. D. Knight, R. E. Young, J. D. Mihalov, L. A. Young, F. S. Milos, G. Schubert, R. C. Blanchard, and D. Atkinson, Thermal structure of Jupiter's atmosphere near the edge of a 5-micron hot spot in the north equatorial belt, *J. Geophys. Res.* **103**, 22 857–22 890, 1998.

Smoluchowski, R., Internal structure and energy emission of Jupiter, *Nature* **215**, 691–695, 1967.

Stevenson, D. J., Turbulent thermal convection in the presence of rotation and a magnetic field: A heuristic theory, *Geophys. Astrophys. Fluid Dyn.* **12**, 139–169, 1979.

Stevenson, D. J., Saturn's luminosity and magnetism, *Science* **208**, 746–748, 1980.

Stevenson, D. J., Formation of the giant planets, *Plan. Space Sci.* **30**, 755–764, 1982a.

Stevenson, D. J., Interiors of the giant planets, *Ann. Rev. Earth Planet. Sci.* **10**, 257–295, 1982b.

Stevenson, D. J., Reducing the non-axisymmetry of a planetary dynamo and an application to Saturn, *Geophys. Astrophys. Fluid Dyn.* **21**, 113–127, 1982c.

Stevenson, D. J., Anomalous bulk viscosity of two-phase fluids and implications for planetary interiors, *J. Geophys. Res.* **88**, 2445–2455, 1983a.

Stevenson, D. J., Planetary magnetic fields, *Prog. Physics* **46**, 555–557, 1983b.

Stevenson, D. J. and N. W. Ashcroft, Conduction in fully ionized liquid metals, *Phys. Rev. A* **9**, 782–789, 1974.

Stevenson, D. J. and E. E. Salpeter, Interior models of Jupiter, in *Jupiter*, T. Gehrels (ed), University of Arizona Press, pp. 85–112, 1976.

Stevenson, D. J. and E. E. Salpeter, The dynamics and helium distribution in hydrogen–helium fluid planets, *ApJS* **35**, 239–261, 1977a.

Stevenson, D. J. and E. E. Salpeter, The phase diagram and transport properties for hydrogen–helium fluid planets, *ApJS* **35**, 221–237, 1977b.

Trafton, L. M., Model atmospheres of the major planets, *ApJ* **147**, 765–781, 1967.

Von Zahn, U., D. M. Hunten, and G. Lehmacher, Helium in Jupiter's atmosphere: Results from the *Galileo* probe helium interferometer experiment, *J. Geophys. Res.* **103**, 22 815–22 830, 1998.

Weir, S. T., A. C. Mitchell, and W. J. Nellis, Metallization of fluid molecular hydrogen at 140 GPa (1.4 Mbar), *Phys. Rev. Lett.* **76**, 1860–1863, 1996.

Wigner, E. and H. B. Huntington, On the possibility of a metallic modification of hydrogen, *Jour. Chem. Phys.* **3**, 764–770, 1935.

Zharkov, V. N., *Interior Structure of the Earth and Planets* (Revised and enlarged edition), Harwood Academic, 1986.

Zharkov, V. N. and T. V. Gudkova, Models of giant planets with a variable ratio of ice to rock, *Annal. Geophys.* **9**, 357–366, 1991.

Zharkov, V. N. and V. P. Trubitsyn, Determination of the equation of state of the molecular envelopes of Jupiter and Saturn from their gravitational moments, *Icarus* **21**, 152–156, 1974.

Zharkov, V. N. and V. P. Trubitsyn, *Physics of Planetary Interiors*, Pachart, 1978.